RAS 5214 72-22-ISFSI — Applicant Exhibit LL — Rec'd 4/29/02

Geomatrix Evaluation of Spatial and Temporal Variation of Ground Motions for the Private Fuel Storage Facility, Skull Valley, Utah

A. Estimate of the Angle of Incidence and Its Effect on Storage Pad Response

It is standard calculation in seismology to obtain the ray path for a seismic body wave traveling from a point source at depth to a site on the surface. The primary ray path is one that minimizes the travel time from the point source to the site. The minimum travel time ray path also obeys Snell's law in that the ratio of the sine of the incidence angle, i_i, at a layer boundary to the velocity within the layer, V_i, is constant all along the ray path:

$$\frac{\sin(i_i)}{V_i} = \text{constant}$$

We have applied this approach to computing the angle of incidence at the surface for waves originating on the primary sources of hazard to the PFS site, the Stansbury and East faults. Figure 1 shows the relationship of the PFS site to the two faults (using the central estimate of fault dip of 55°). The strain-compatible site velocity profile is shown on Figure 4 of Geomatrix Calculation 05996.02-G(PO18)-2 (Rev. 1) and is listed in Table 1 with layer thickness and velocities converted to meters and meters/second, respectively. We have calculated the ray paths for three points on the fault plane that span the expected depth range for release of most of the seismic energy (depths of 5 to 15 km). Table 2 lists the computed angles of incidence for this velocity model and the six point sources shown on Figure 1.

Table 1
Skull Valley Mean Strain-Compatible Velocity Profile
From Figure 4 of Calculation 05996.02-G(PO18)-2, Rev 1

Layer Thickness (m)	Total Thickness (m)	Layer Shear Wave Velocity (m/s)
1.524	1.524	456.3
1.524	3.048	126 4
0.610	3.658	189.7
1.829	5.486	237.4
2.438	7.925	231.7
2.743	10.668	249.4
4.572	15.240	291.3
12.192	27.432	523.1
64.008	91.44	883.9
60.960	152.40	1051.6
60.960	213.36	1204.0
1,186.64	1400	1,950
18,600	20000	3,400

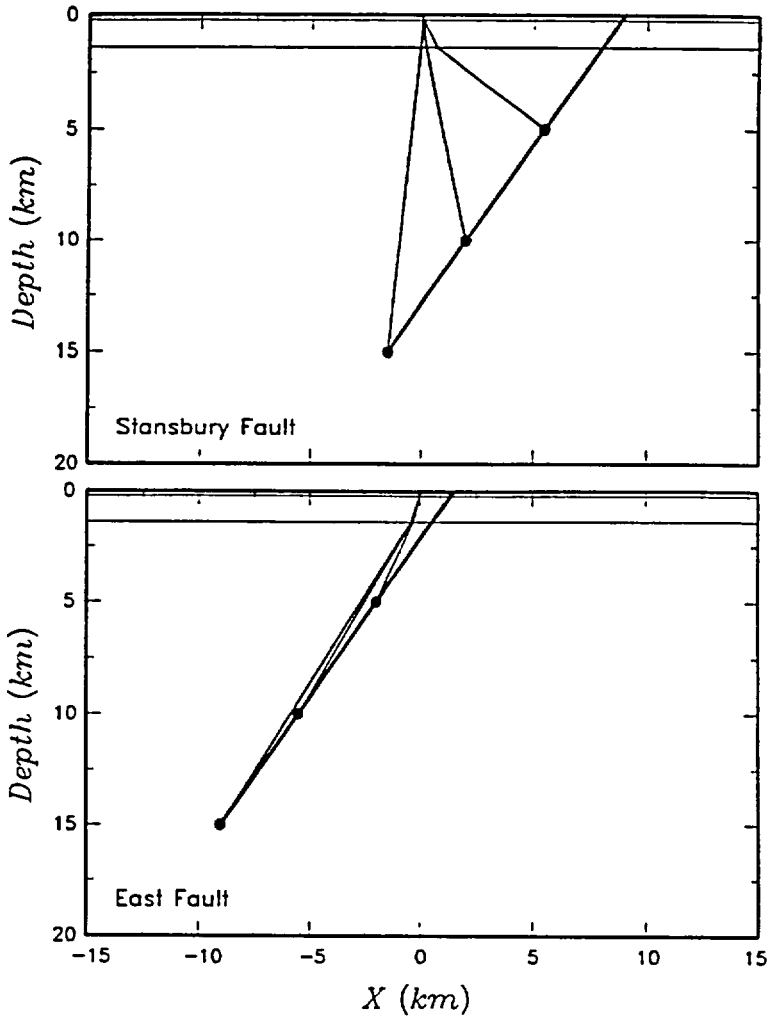

Figure 1 Example ray paths for seismic waves from fault ruptures in Skull Valley

Table 2
Surface Layer Angles of Incidence for Skull Valley Velocity Model (Table 1)

Fault	Source Point Location		Surface Layer Angle of Incidence (°)
	Depth (km)	Surface Distance (km)	
Stansbury fault	5	5.5	6.1
	10	2	1.6
	15	1.5	0.8
East fault	5	-2	3.1
	10	-5.5	3.9
	15	-9	4.1

The ray tracing analysis described above is for an infinite frequency wave, one that will be able to react to all of the layer velocity changes. The velocity model listed in Table 1

68222

contains thin layers near the surface, which will most influence the response of the site to high frequency waves. The site response to lower frequency waves can be modeled by replacing the detailed velocity model (Table 1) with thicker layers of uniform velocity. For example, the fundamental frequency of the 700-foot thick sedimentary sequence in Skull Valley is approximately 1 Hz. Thus, the response of the site to 1-Hz waves can be approximated using a single 700-foot thick layer with a uniform velocity equal to the average (harmonic mean) of the velocities of all of the layers to a depth of 700 feet (213.4 meters). If one uses this simpler velocity representation to assess the direction of wave propagation, the thicker single layer with uniform velocity will result in larger angles of incidence at the surface than those listed in Table 2.

Analysis of the time-histories of response of the casks (see Section C) indicates that the frequencies of interest are in the range of 1 to 5 Hz. To assess potential ray paths for waves in this frequency range, simplified velocity models were constructed by combining layers of the detailed model listed in Table 1 to produce layers with fundamental frequencies near the target frequency. Table 3 lists these simplified velocity models representative of layers with predominant frequencies of 5, 2.5, and 1 Hz. Table 4 lists the computed angles of incidence for these simplified models.

Table 3
Simplified Skull Valley Velocity Model for 5 Hz Waves

Layer Thickness (m)	Total Thickness (m)	Layer Shear Wave Velocity (m/s)
10.668	10.668	223.0
16.764	27.432	429.8
12.192	27.432	523.1
64.008	91.44	883.9
60.960	152.40	1051.6
60.960	213.36	1204.0
1,186.64	1400	1,950
18,600	20000	3,400

Simplified Skull Valley Velocity Model for 1 Hz Waves

Layer Thickness (m)	Total Thickness (m)	Layer Shear Wave Velocity (m/s)
213.35	213.35	832.1
1,186.64	1400	1,950
18,600	20000	3,400

Table 4
Surface Layer Angles of Incidence for
Simplified Skull Valley Velocity Models Listed in Table 3

Fault	Source Point Location		Surface Layer Angle of Incidence (°) for Simplified Velocity Model for Frequency:	
	Depth (km)	Surface Distance (km)	1 Hz	5 Hz
Stansbury fault	5	5.5	11.3	3.0
	10	2	2.9	0.8
	15	1.5	1.9	0.4
East fault	5	-2	5.9	1.6
	10	-5.5	7.2	1.9
	15	-9	7.5	2.0

The velocity models listed in Table 3 assume horizontal layer boundaries. Seismic line 2 obtained by Geosphere Midwest [1997, Figure 4.6, reprinted on p. 2 of Attachment A of Geomatrix Calculation 05996.02-G(PO18)-2 (Rev. 1)] shows that the bedrock surface beneath the site dips gently down to the east with a 200-ft drop over the ~3,000-ft length of the profile. Table 5 lists the angles of incidence computing using a Tertiary-bedrock boundary with a 4° dip down to the east. The sloping bedrock changes the incidence angles by a few degrees at most.

Table 5
Surface Layer Angles of Incidence for
Simplified Skull Valley Velocity Models Listed in Table 3 Including 4° Bedrock Slope

Fault	Source Point Location		Surface Layer Angle of Incidence (°) for Simplified Velocity Model for Frequency:	
	Depth (km)	Surface Distance (km)	1 Hz	5 Hz
Stansbury fault	5	5.5	8.9	2.7
	10	2	0.6	0.5
	15	1.5	0.8	0.1
East fault	5	-2	8.2	1.9
	10	-5.5	9.5	2.2
	15	-9	9.9	2.3

The above results indicate that the expected angles of incidence at the surface for seismic waves originating from large-magnitude earthquake ruptures on the adjacent faults is small, typically less than 10° from vertical. Thus, the proximity of the site to the major active faults does not result in high angle of incidence waves measured from vertical (i.e., low angle measured from horizontal) and the assumption of vertically propagating waves is reasonable for the site.

Inclined waves will result in a difference in arrival time for waves at two adjacent points. The time difference for two points separated by distance w measured in the direction toward the source is approximately equal to $w \sin(i_1)/V_1$, where the subscript 1 refers to the surface layer. The storage pads have a width of 30 feet in the east-west (fault-normal) direction. Using this value for w, the incidence angles listed in Table 4 together with the velocities listed in Table 3, one obtains time differences on the order of 0.001 to 0.002 seconds. These time differences are much smaller than the minimum time step of the time histories developed for the site (0.005 seconds) and would affect only very high frequency motions above the highest ground motion frequency of interest (50 Hz). Thus, the very small time difference for wave arrivals would have negligible effect on the analysis.

The effects of the low incident angles on the input motion (measured from vertical) to the pads as compared to vertically propagating waves also can be examined based on the work by Luco (1976) and Wong and Luco (1978). The controlling parameters are the normalized frequency, $a_0 = \omega a/\beta$, (where ω is the angular frequency in radians/sec, a is the equivalent radius of the pad, and β is the shear-wave velocity of the near-surface layer); and the ratio of shear-wave velocity to apparent wave velocity, β/c (equivalent to the sine of the angle of incidence). The equivalent pad radius = $\sqrt{30 \times 67/\pi}$ = 25.3 ft = 7.7 m. For a 5-Hz wave, the largest incident angle of 3° results in $\beta/c = \sin(3°) = 0.05$. From Table 3, β = 223 m/s, resulting in $a_0 = 1.1$. For this case, Luco (1976, Fig. 3) indicates that an SH-wave would induce a torsional motion equivalent to an additional horizontal motion of about 3 percent of the amplitude of the free-field motion at the edge of the pad. For a 1-Hz wave, the largest incident angle of 11.3° results in $\beta/c = \sin(11.3°) = 0.2$. From Table 3, β = 832 m/s, resulting in $a_0 = 0.06$. For this case Luco (1976, Fig. 3) indicates less than 1 percent additional motion. Accompanying this is a slight reduction in the translation motion.

Wong and Luco (1978, Fig. 4, 5, 6, and 7) show the effect of inclined P/SV waves as a function of a_0 and β/c. The parameter a is now defined as the half-width of a square mat = $\sqrt{30 \times 67}/2$ = 22.4 ft = 6.8 m. For 5-Hz waves, $a_0 = 1.0$ and β/c is very small (0.05). For this case, Figures 4 through 7 of Wong and Luco (1978) indicate that the response is generally within 5 percent of that for vertical waves. For 1-Hz motions, a_0 is very small (0.06), and the response is again within 5 percent of that for vertical waves.

Thus, it can be concluded that additional rocking and torsional motion of the pad caused by inclined incident waves at the small angles listed in Tables 2 and 4 is insignificant compared to the motion caused by the vertically propagating waves.

B. Estimate of the Degree of Spatial Incoherence for Storage Pads

The degree of spatial variation in ground motions can be measured by the spatial coherency of ground motion. Abrahamson et al. (1991) developed an empirical model for spatial coherency using data from the Lotung LSST strong motion array in Taiwan. They define a model for the "lagged" coherency, $\gamma(f,\xi)$, which models the effects of scattering on ground motions; and a model for the "unlagged" coherency, $\gamma_U(f,\xi,\xi_r)$, which includes wave passage effects due to inclined waves. Their relationship for unlagged coherency is given by the expression:

$$\gamma_U(f,\xi,\xi_r) = \gamma(f,\xi)\cdot\phi(f,\xi_r)$$

in which

$$\gamma(f,\xi) = \tanh[(2.535 - 0.0118\xi)\{\exp(f(-0.155 - 0.000837\xi)) + \tfrac{1}{3}f^{-0.878}\} + 0.35]$$

and

$$\phi(f,\xi_r) = \frac{\cos(2\pi\cdot 0.00037 f\xi_r)}{1+(f/19)^4}$$

where f is frequency, ξ is the separation distance, and ξ_r is the separation distance measured along the path toward the source (i.e. fault-normal). The term $\phi(f, \xi_r)$ represents incoherency due to the wave-passage effect. In the east-west direction $\xi = \xi_r = 9.14$ meters. For this direction one obtains the following values for the frequency range of interest:

Table 6
Empirical Coherency for East-West Direction

Frequency (Hz)	$\gamma(f,\xi)$	$\phi(f, \xi_r)$	$\gamma_U(f,\xi,\xi_r)$
1	1.00	1.00	1.00
2.5	0.99	1.00	0.98
5	0.95	0.99	0.94

In the north-south direction, $\xi = 20.4$ meters and $\xi_r = 0$ (direction parallel to fault). For this direction one obtains the following values:

68226

Table 7
Empirical Coherency for North-South Direction

Frequency (Hz)	$\gamma(f,\xi)$	$\phi(f,\xi_r)$	$\gamma_U(f,\xi,\xi_r)$
1	1.00	1.00	1.00
2.5	0.98	1.00	0.98
5	0.94	1.00	0.93

As indicated by Abrahamson et al. (1991), the above values represent the fraction of the power in the ground motions that can be represented by a vertically propagating plane wave. The values in the table indicate that for the small pad size of interest, nearly all of the power in the ground motions can be represented by a vertically propagating plane wave.

In addition, Abrahamson et al. (1991) show in their Figure 10 the residuals between observed data and their empirical model for two epicentral distance ranges, $\leq$ 15 km and $\geq$40 km. The mean residuals for the two distance ranges oscillate about each other and the authors conclude that the data do not indicate a clear dependence of spatial coherency on distance from the source. On this basis we conclude that proximity to the major active faults does not require special evaluation of the effects of spatial variation.

68227

C. Evaluation of Frequency Range of Importance to Cask Response

The frequency range of importance to cask response was determined by analysis of response time histories obtained at the top of the cask for the worst cases (i.e., a 2-cask system with coefficients of friction of 0.8 and 0.2). This evaluation is based examination of the Fourier amplitude of the output motions computed at the top of the cask and the ratio of the Fourier amplitude between the output motion and the input motion for the two cases. Time histories of the cask response presented in Appendix A show that the tipping and sliding of the cask occurs primarily within the time window of 4 to 7 seconds. Fourier spectra of the velocity time histories of the time window from 4 to 7 seconds for both output and input motions and the spectral ratio of the Fourier amplitude of the output motion divided by those for the input motion are shown on Figures 2 to 5. Both the Fourier spectra of the output motions and the spectral ratios shown on Figures 2 to 5 indicate that the frequency range of peak cask response is between 1 and 5 Hz.

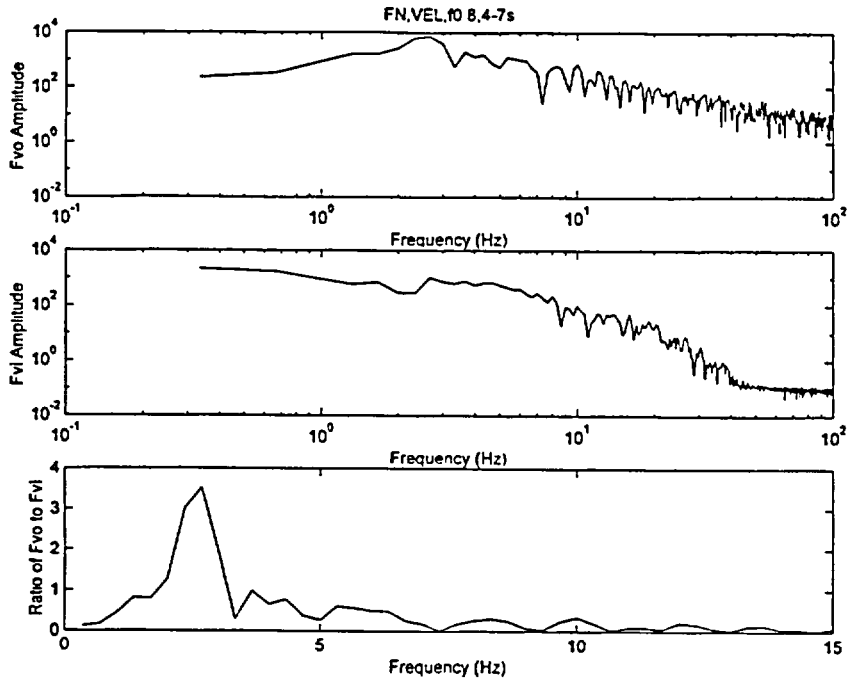

Figure 2: Fourier amplitudes of Cask 2 output motion (top plot), input motion (middle plot), and ratio of Fourier amplitudes (output/input) for motion in X-direction (fault-normal), coefficient of friction = 0.8 and time window 4 to 7 seconds.

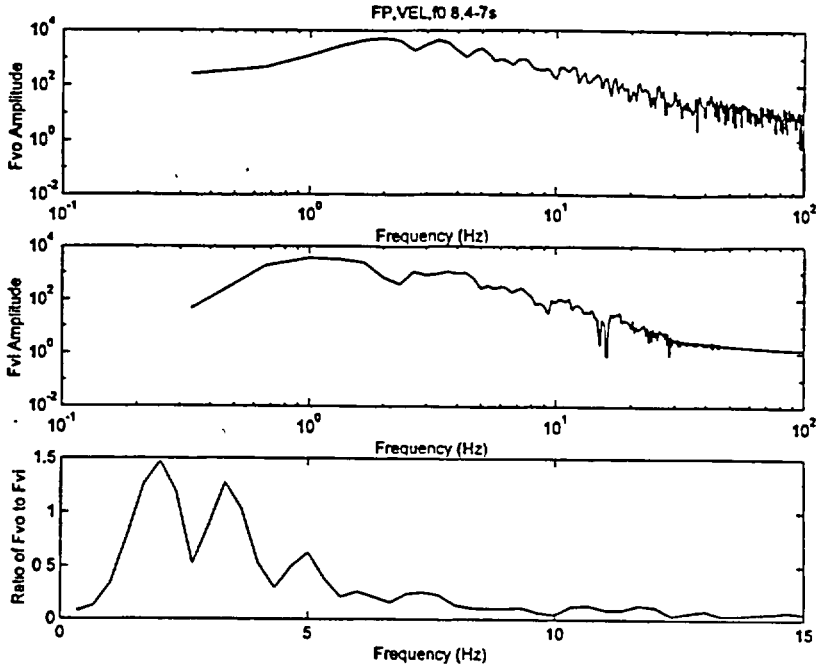

Figure 3: Fourier amplitudes of Cask 2 output motion (top plot), input motion (middle plot), and ratio of Fourier amplitudes (output/input) for motion in Y-direction (fault-parallel), coefficient of friction = 0.8 and time window 4 to 7 seconds.

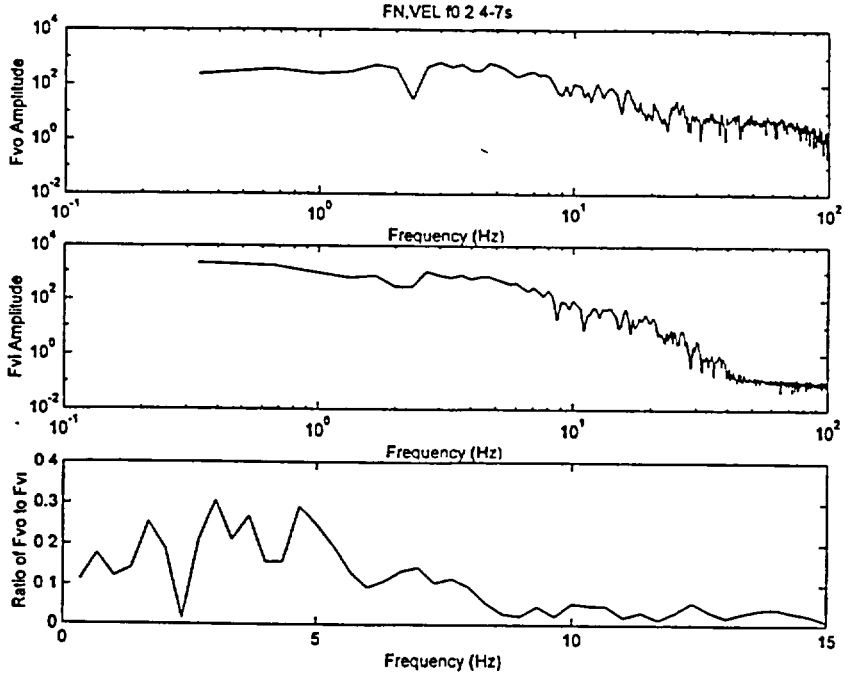

Figure 4: Fourier amplitudes of Cask 2 output motion (top plot), input motion (middle plot), and ratio of Fourier amplitudes (output/input) for motion in X-direction (fault-normal), coefficient of friction = 0.2 and time window 4 to 7 seconds.

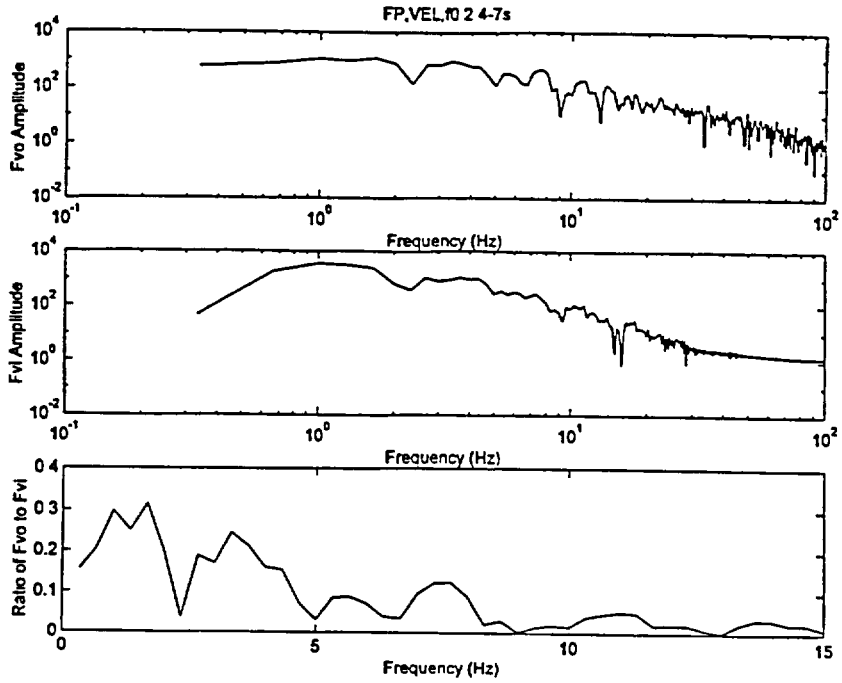

Figure 5: Fourier amplitudes of Cask 2 output motion (top plot), input motion (middle plot), and ratio of Fourier amplitudes (output/input) for motion in Y-direction (fault-parallel), coefficient of friction = 0.2 and time window 4 to 7 seconds.

References

Abrahamson, N.A., J.F. Schneider, and J.C. Stepp, 1991, Empirical spatial coherency functions for application to soil-structure interaction analyses: *Earthquake Spectra*, v. 7, p. 1-27.

Luco, J.E., 1976, Torsional Response of Structures to Obliquely Incident Seismic SH Waves: *Earthquake Engineering and Structural Dynamics*, v. 4, p. 207-219.

Wong, H.L. and Luco, J.E., 1978, Dynamic Response of Rectangular Foundations to Obliquely Incident Seismic Waves: *Earthquake Engineering and Structural Dynamics*, v. 6, p. 3-16.

Appendix A

Time Histories of Cask Response of a Two Cask System For Coefficients of Friction of 0.8 and 0.2

Fig. 1-Cask 1 Disp -X vs. Time cof=0.8 at point 2, file:ck1disp8

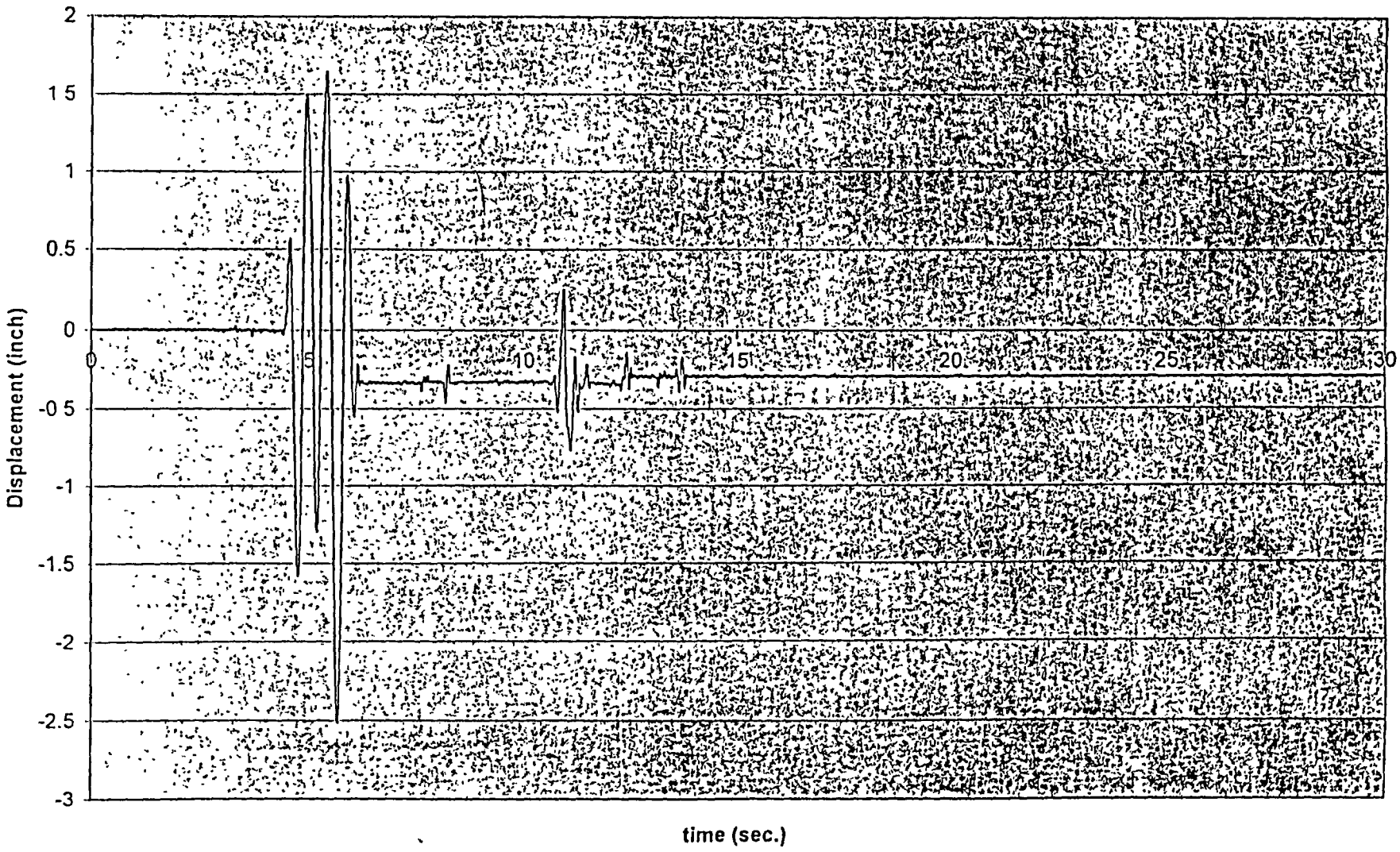

68232

Fig. 2 Cask 1 Disp Y vs Time, cof=0.8 for point 2, file:ck1disp8

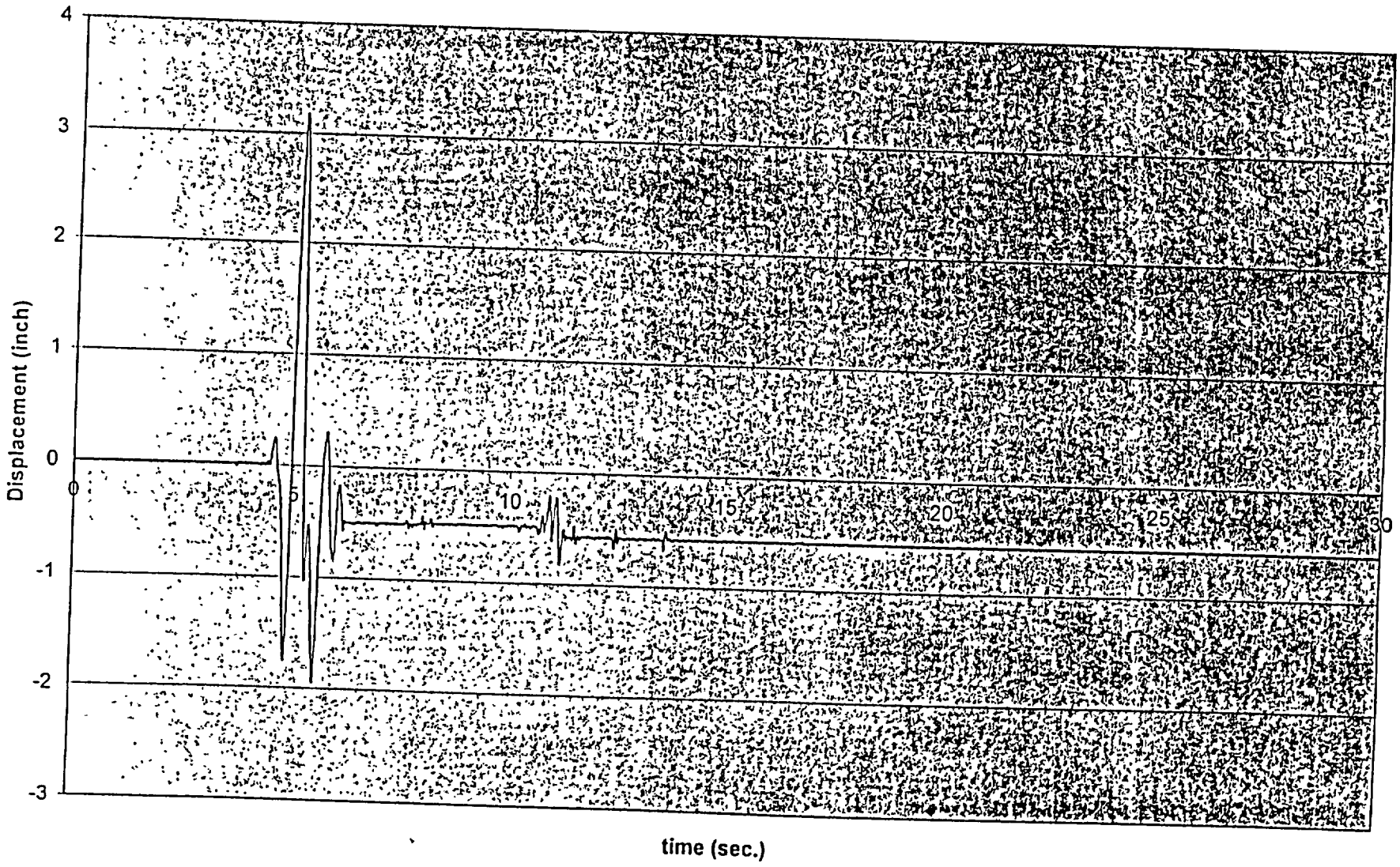

Fig. 3 Cask 1 Velocity x vs. time cof=0.8, file:pfs108

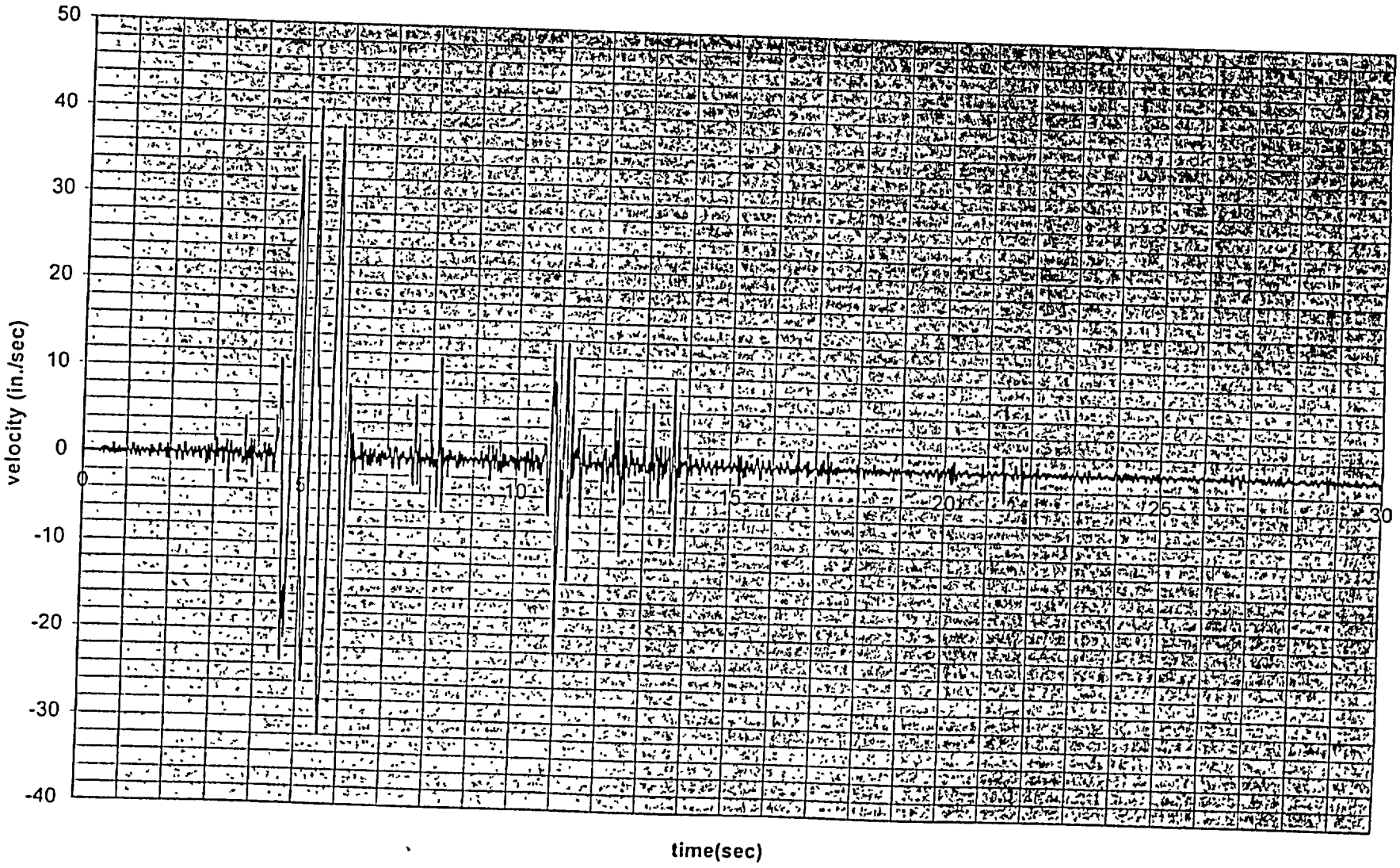

Fig. 4 Cask 1 Velocity Y vs Time cof=0.8, file:pfs108

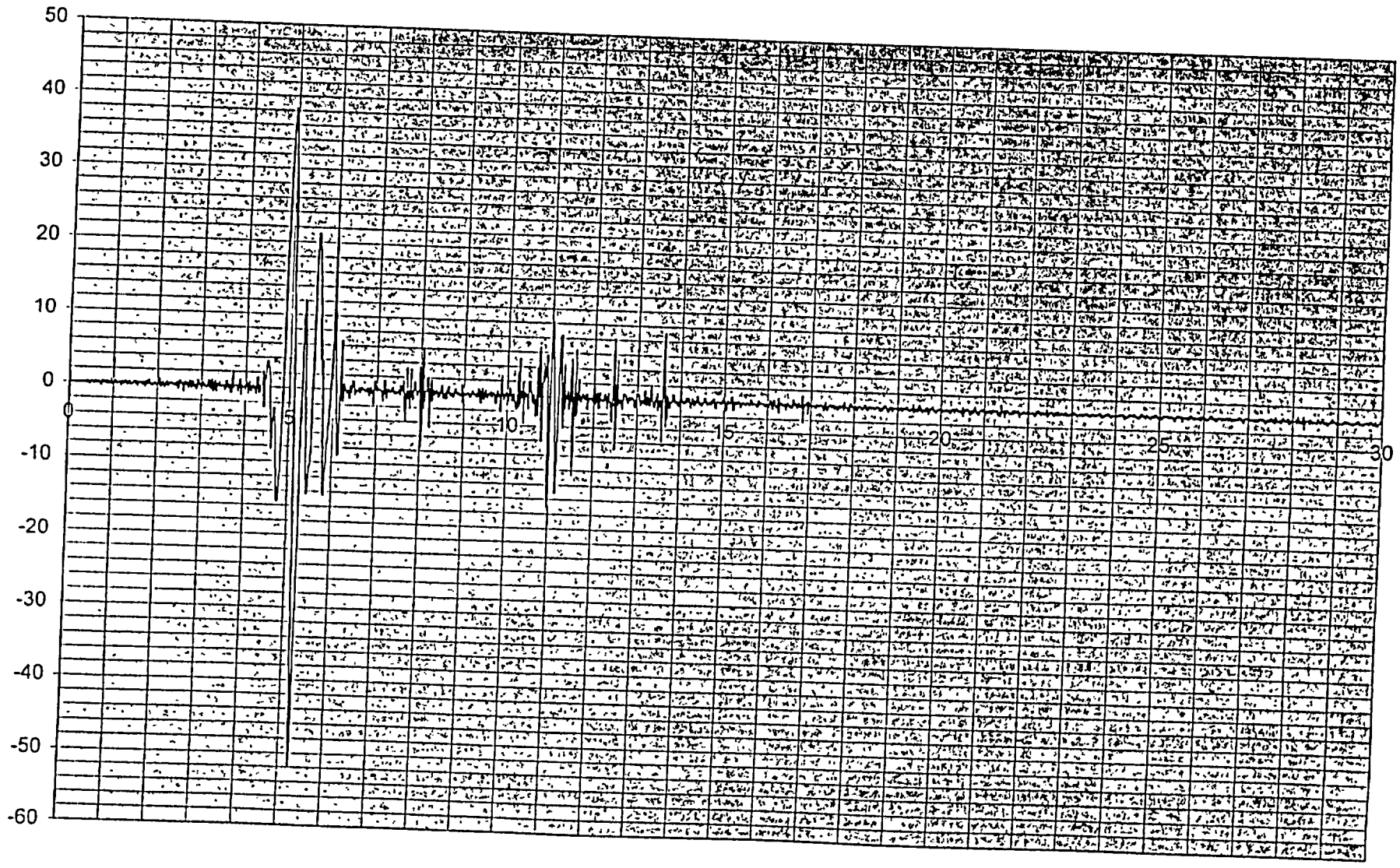

68235

Fig. 5 Cask 1 X accel vs time cof=0.8, file:pfs108

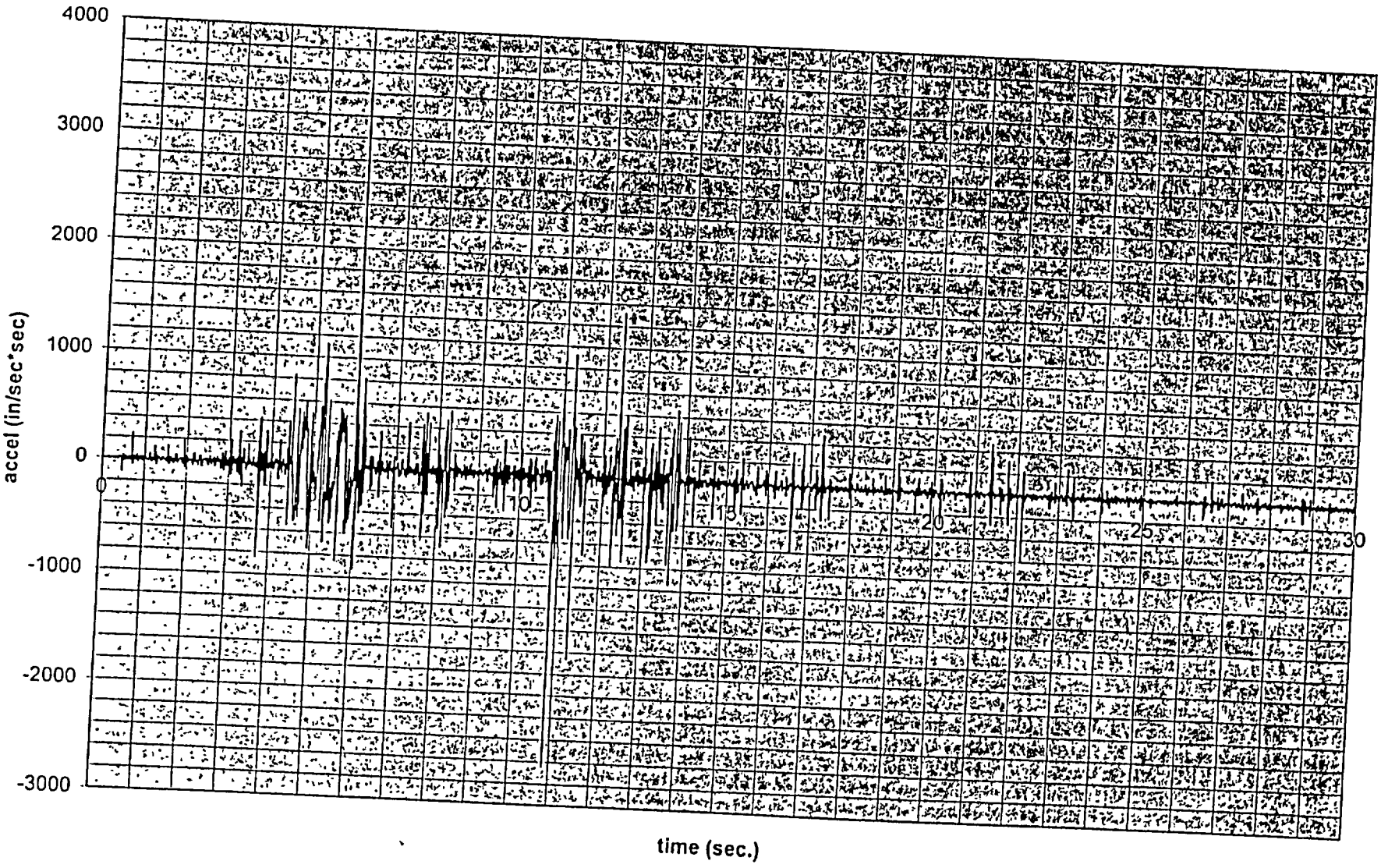

68236

Fig. 6 Cask 1 Accel-Y vs time, cof=0.8, file:pfs108

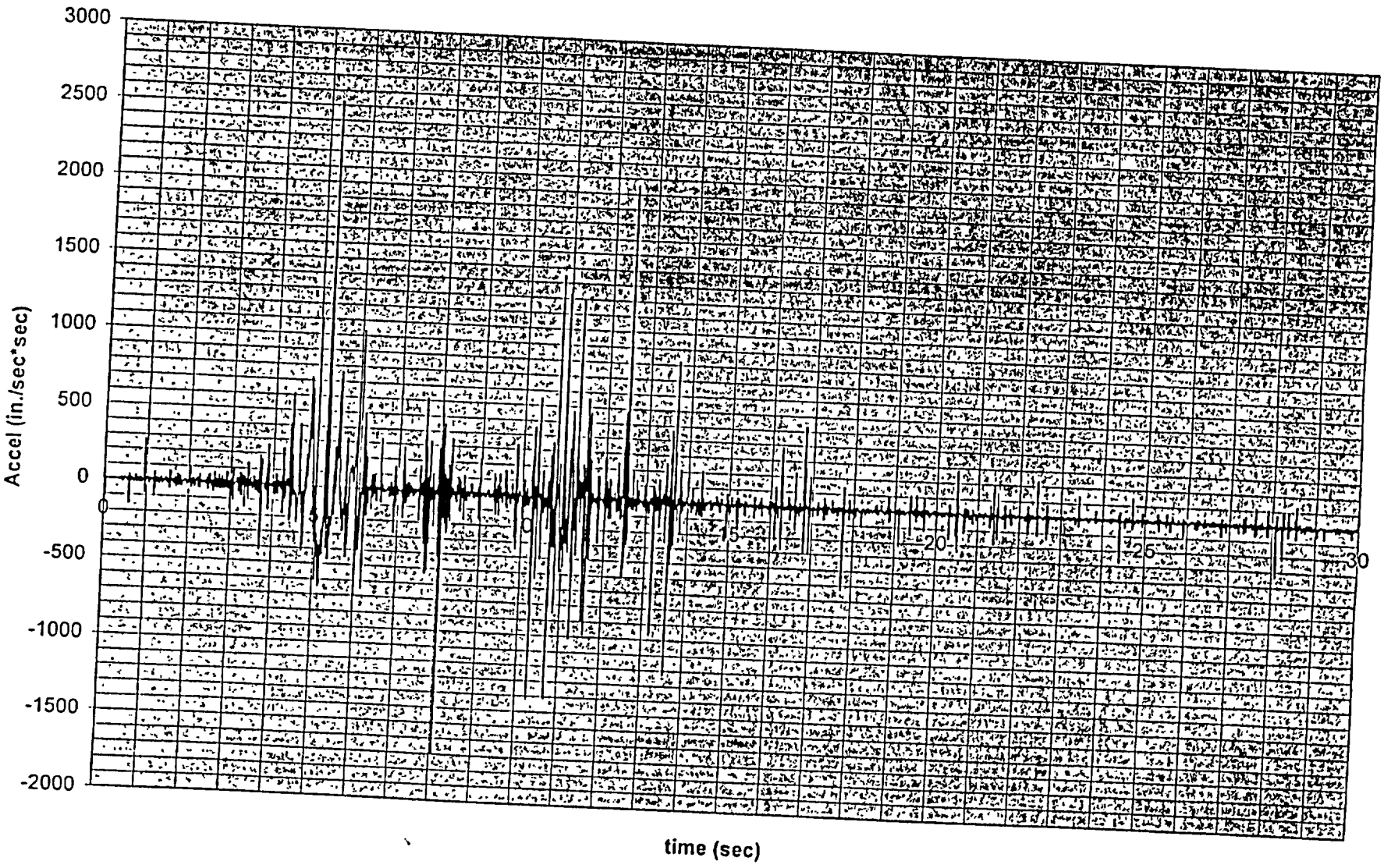

68237

Fig. 7 Cask 2 Disp-X vs Time at point 2, cof=0.8, file:ck2disp8

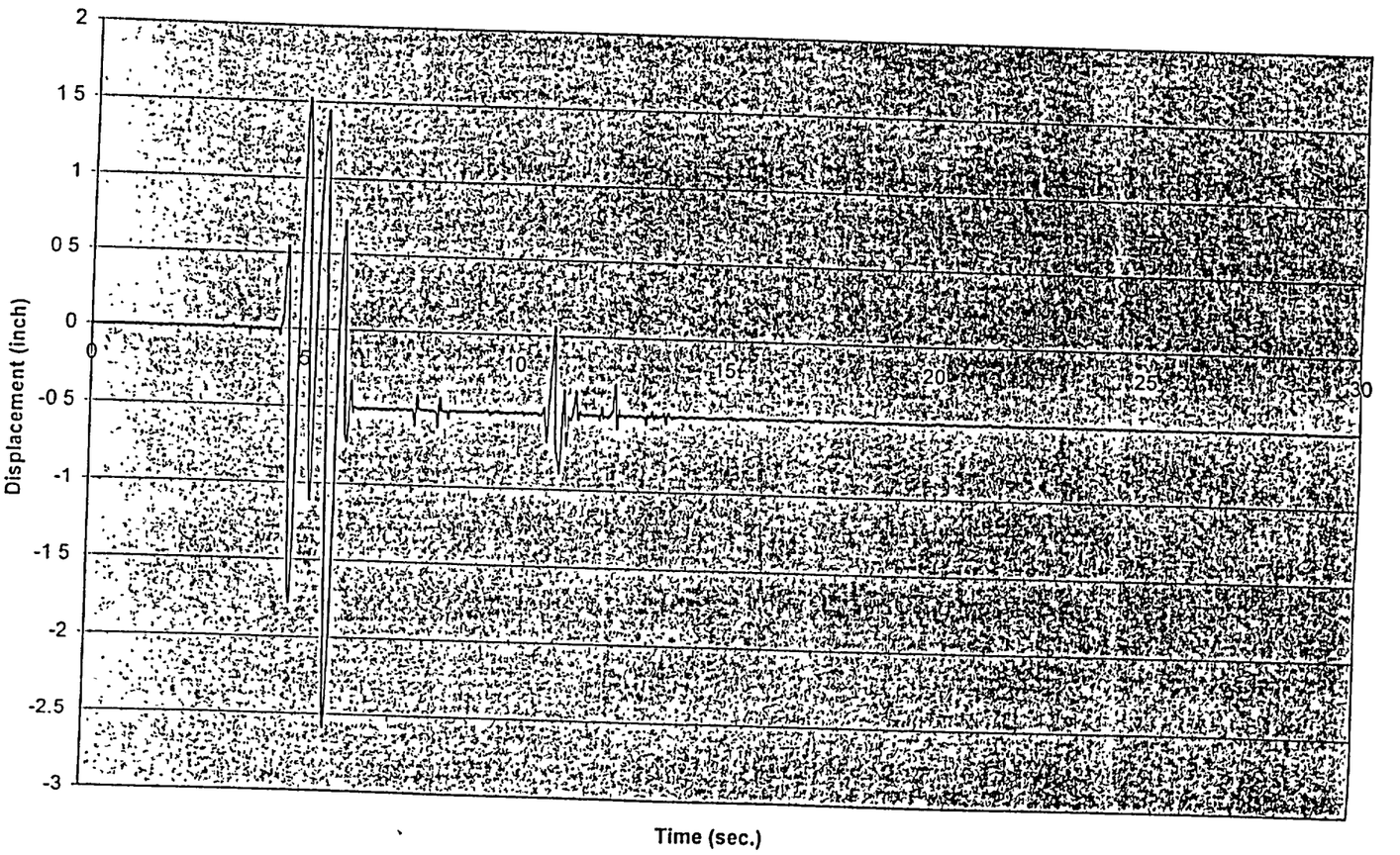

68238

Fig. 8 Cask 2 Disp-Y vs Time at point 2, cof=0.8, file:ck2disp8

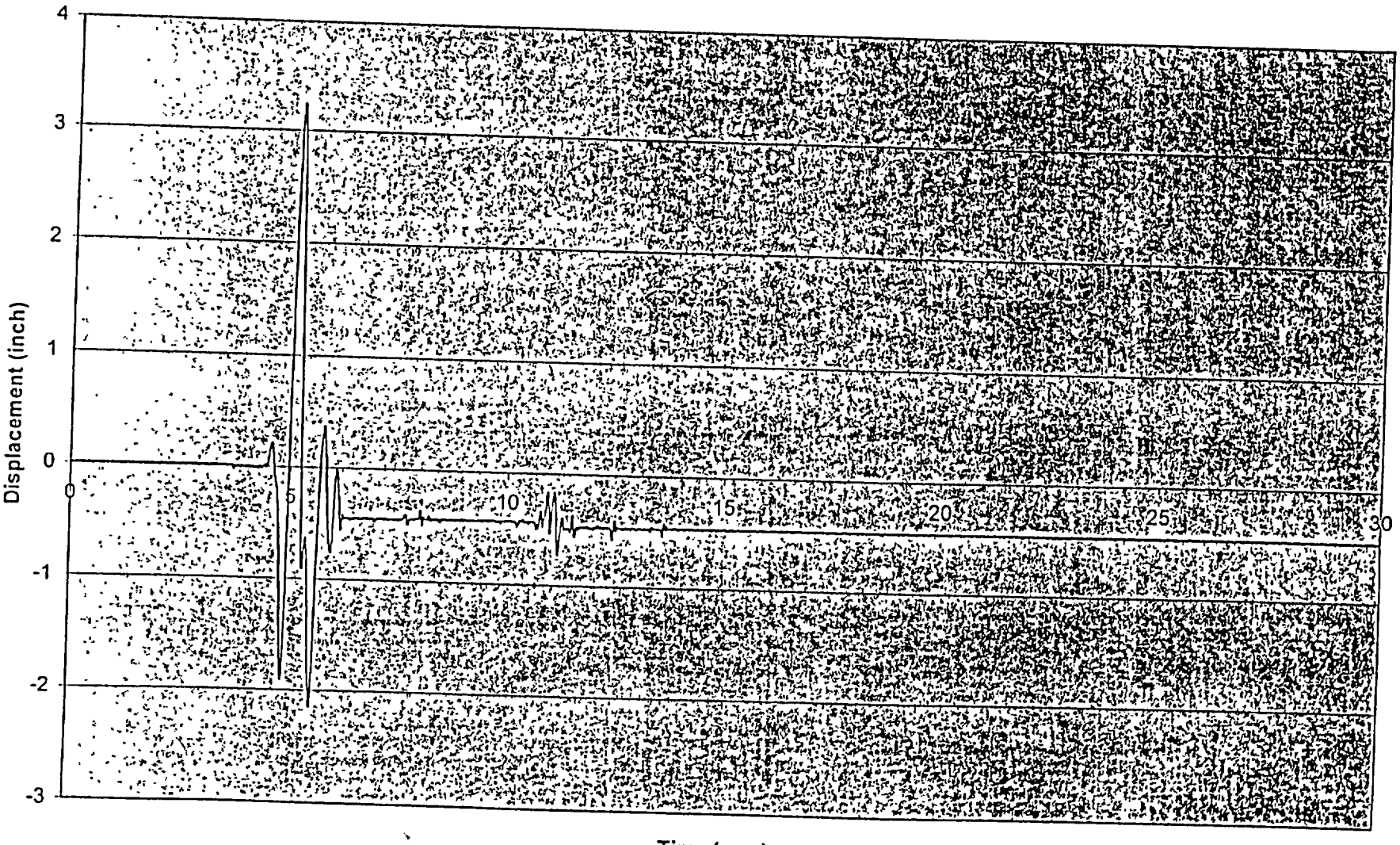

68239

Fig. 9 Cask 2 Velocity X vs Time cof=0.8, file:pfs208

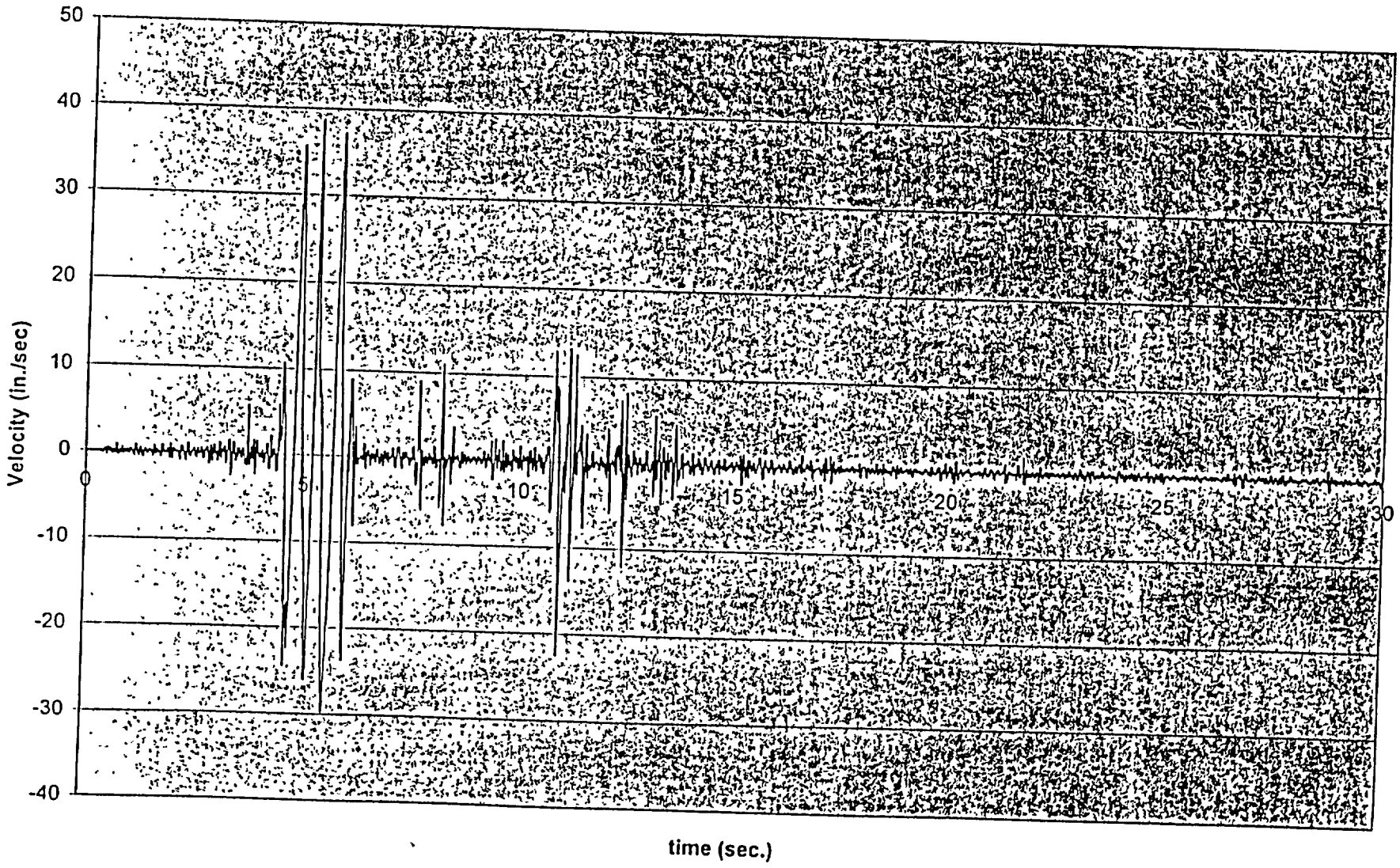

68240

Fig. 10 Cask 2 Velocity Y vs Time cof=0.8, file:pfs208

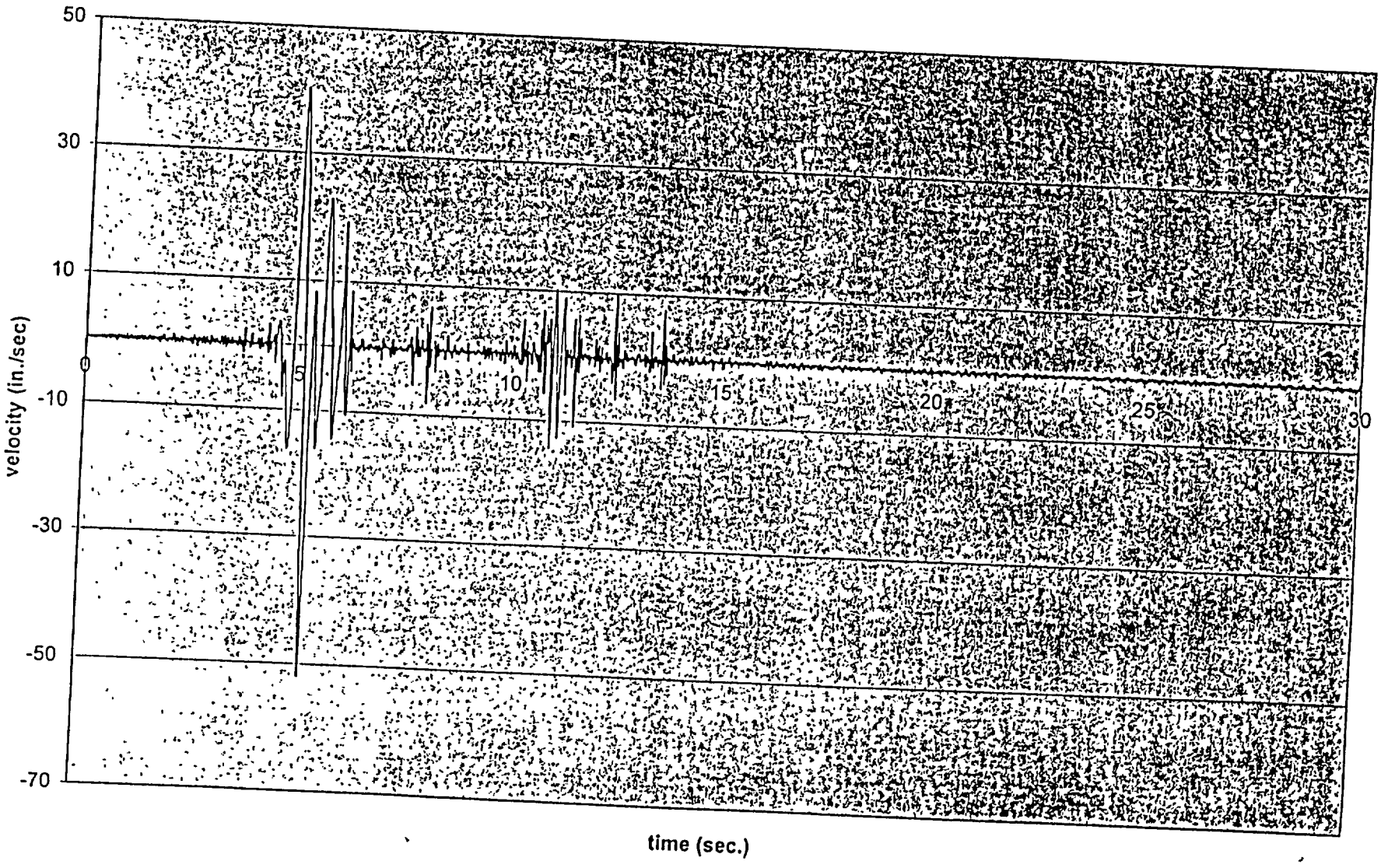

68241

Fig. 11 Cask 2 X Accel Vs Time coef=0.8, file:pfs208

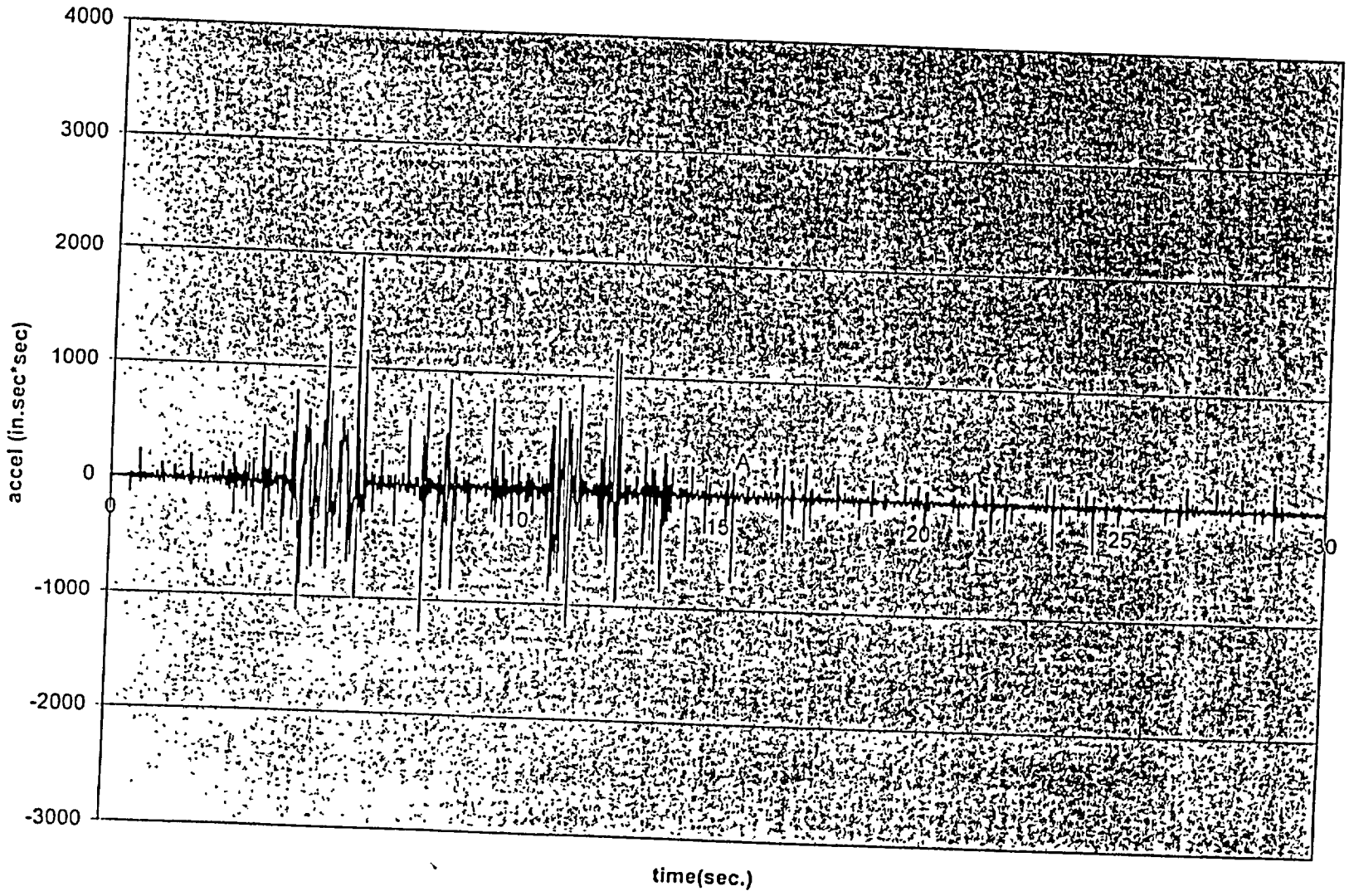

68242

Fig. 12 Cask 2 Y accel vs time coeff=0.8, file:pfs208

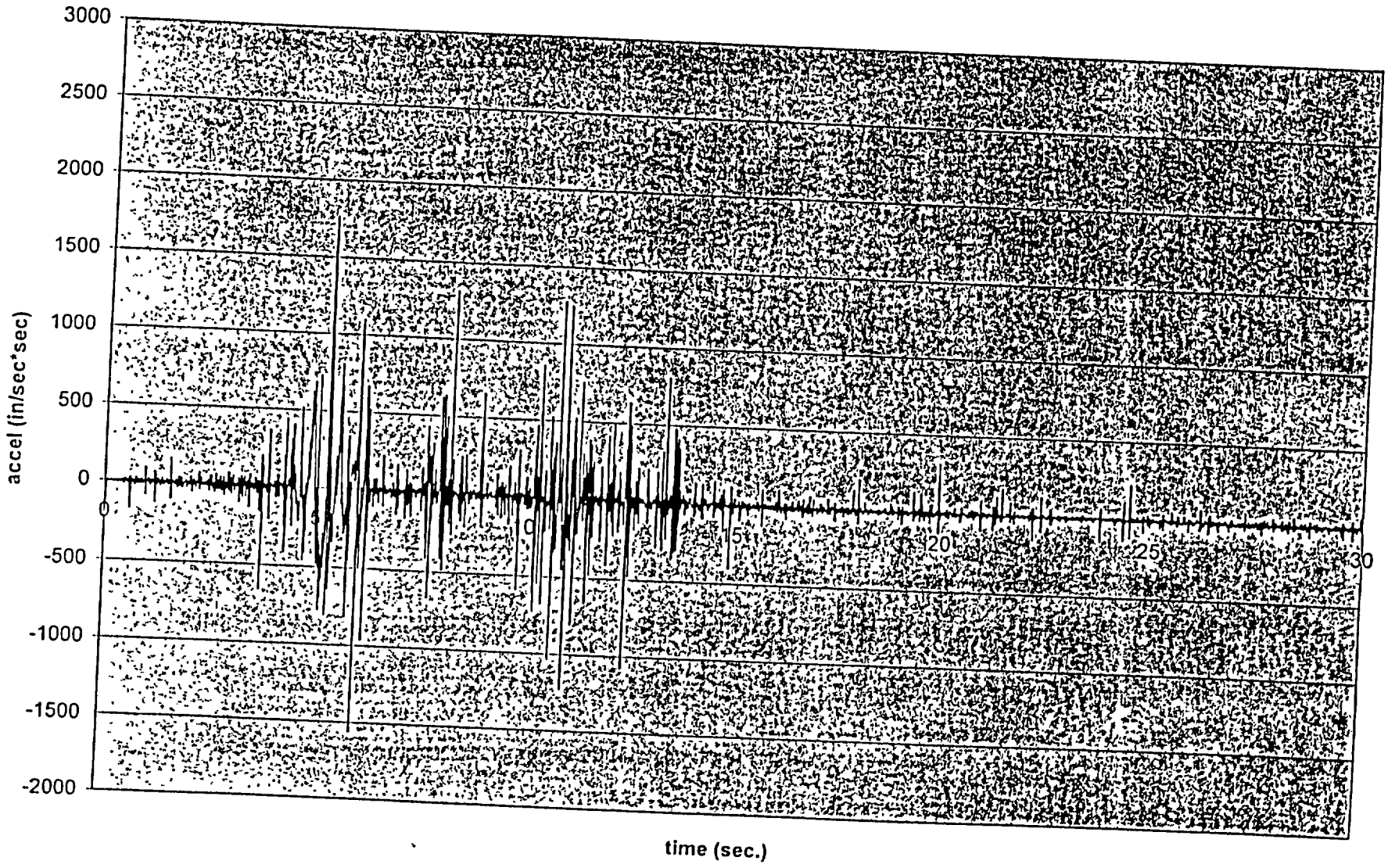

68243

Fig. 13 Cask 1 Disp-x cof=0.2 at point 2, file:ck1disp2

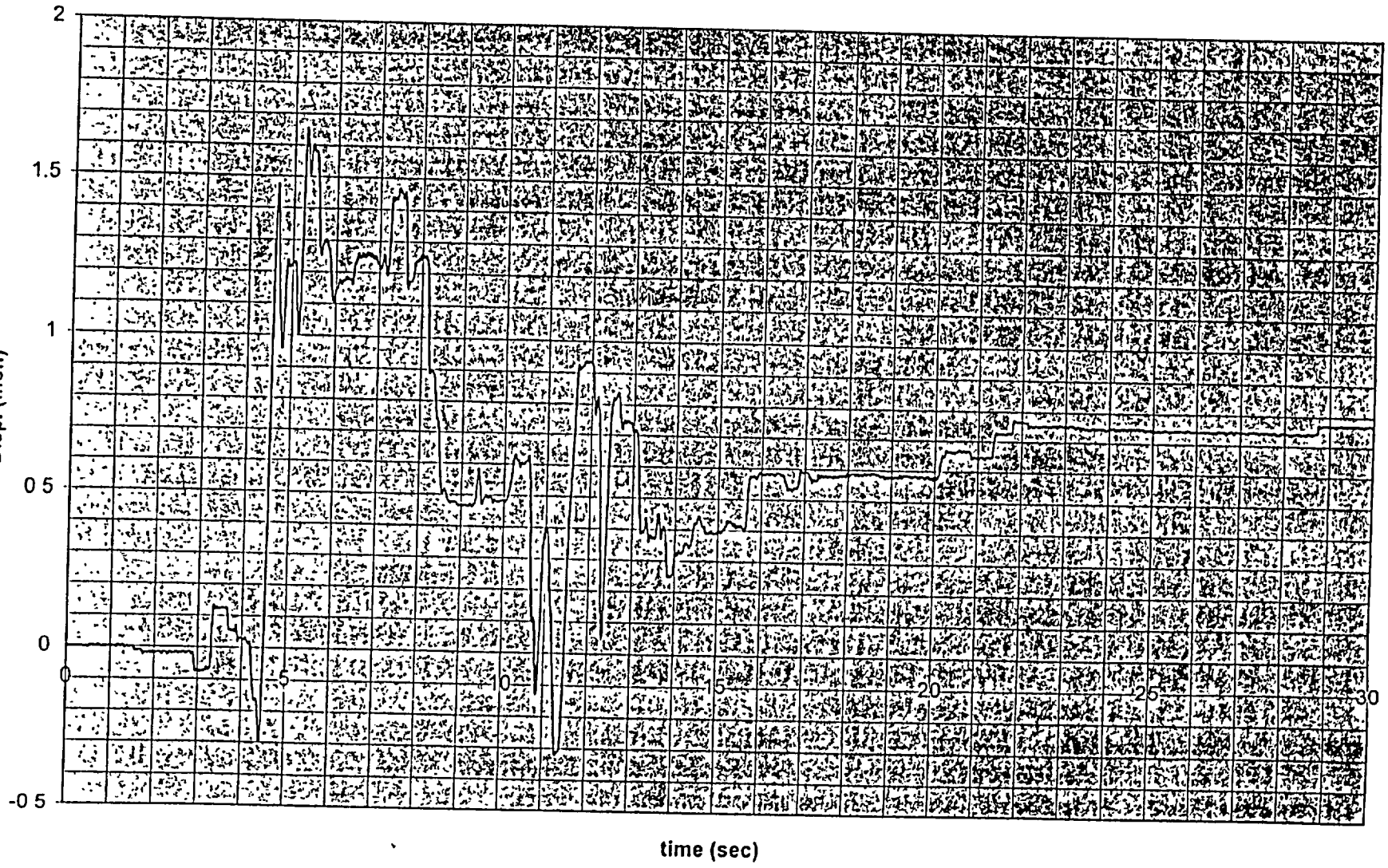

68244

Fig. 14 Cask 1 Disp-Y, COF=0.2 at point 2, file:ck1disp2

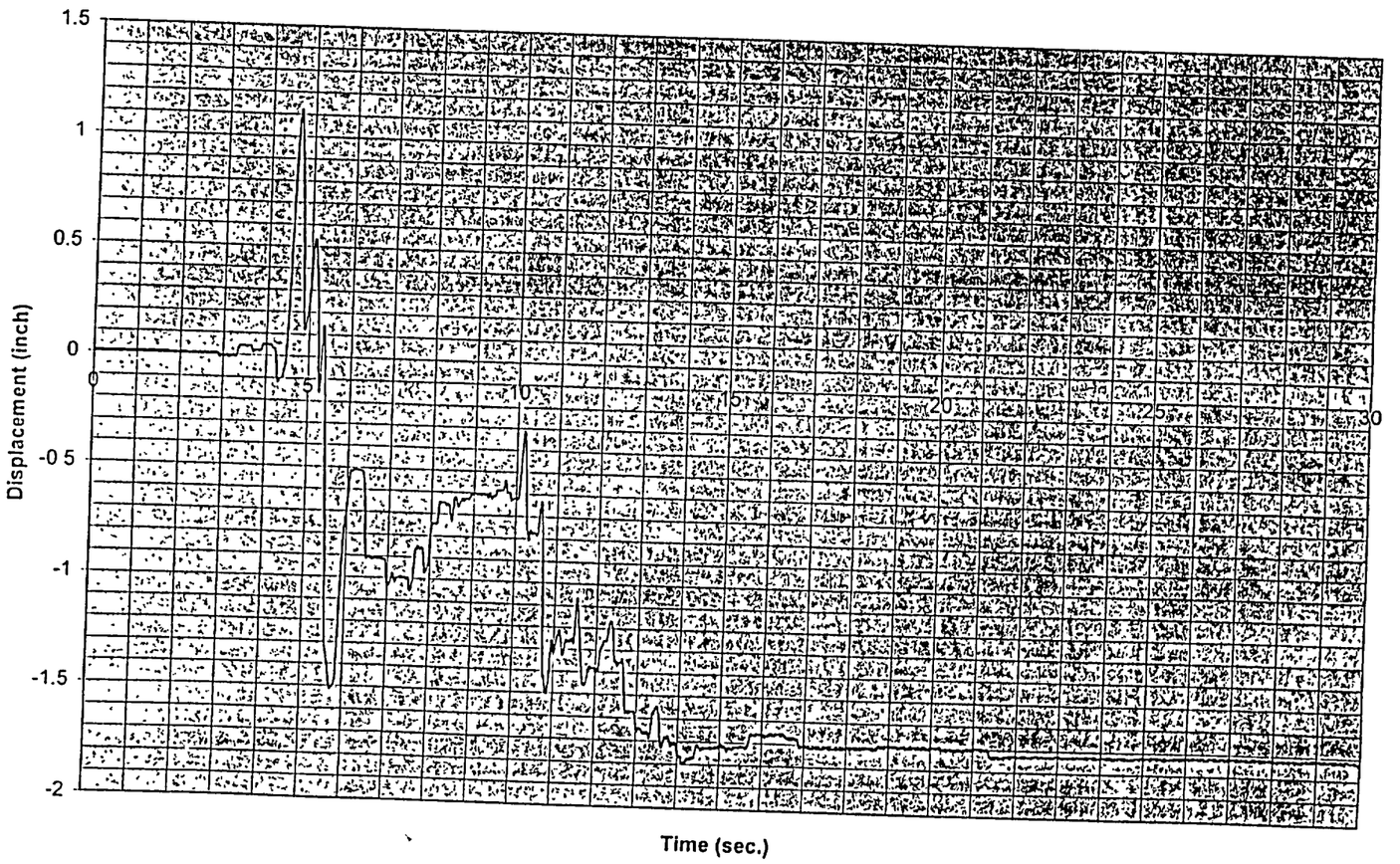

Fig. 15 Cask 1 Vel-X vs Time,Cof=0.2 at point 2, file:pfs102

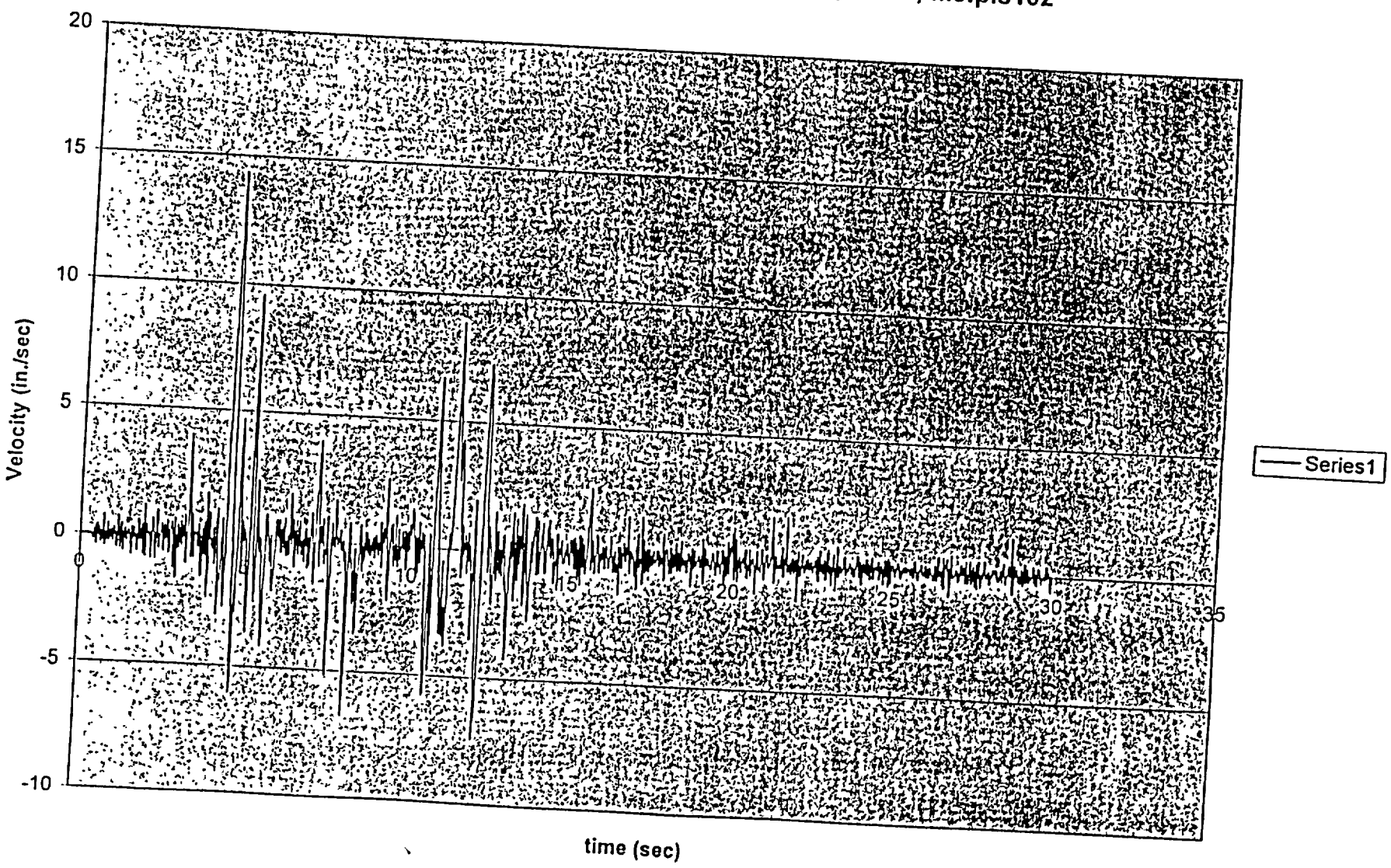

68246

Fig. 16 Cask 1 Vel-Y vs Time,cof=0.2 at point 2, file:pfs102

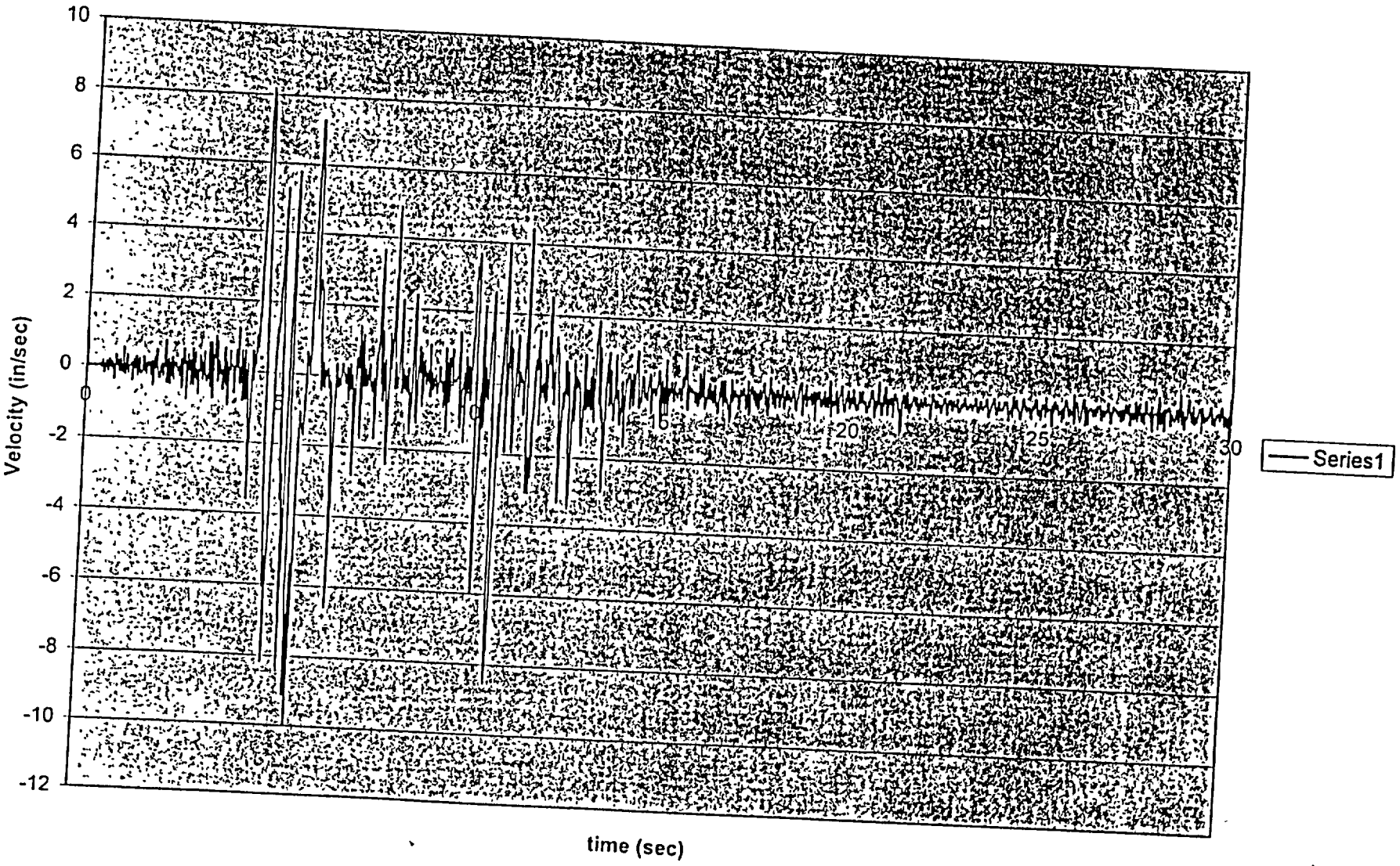

Fig. 17 Cask 1 Accel-X vs Time,cof=0.2 at point 2, file:pfs102

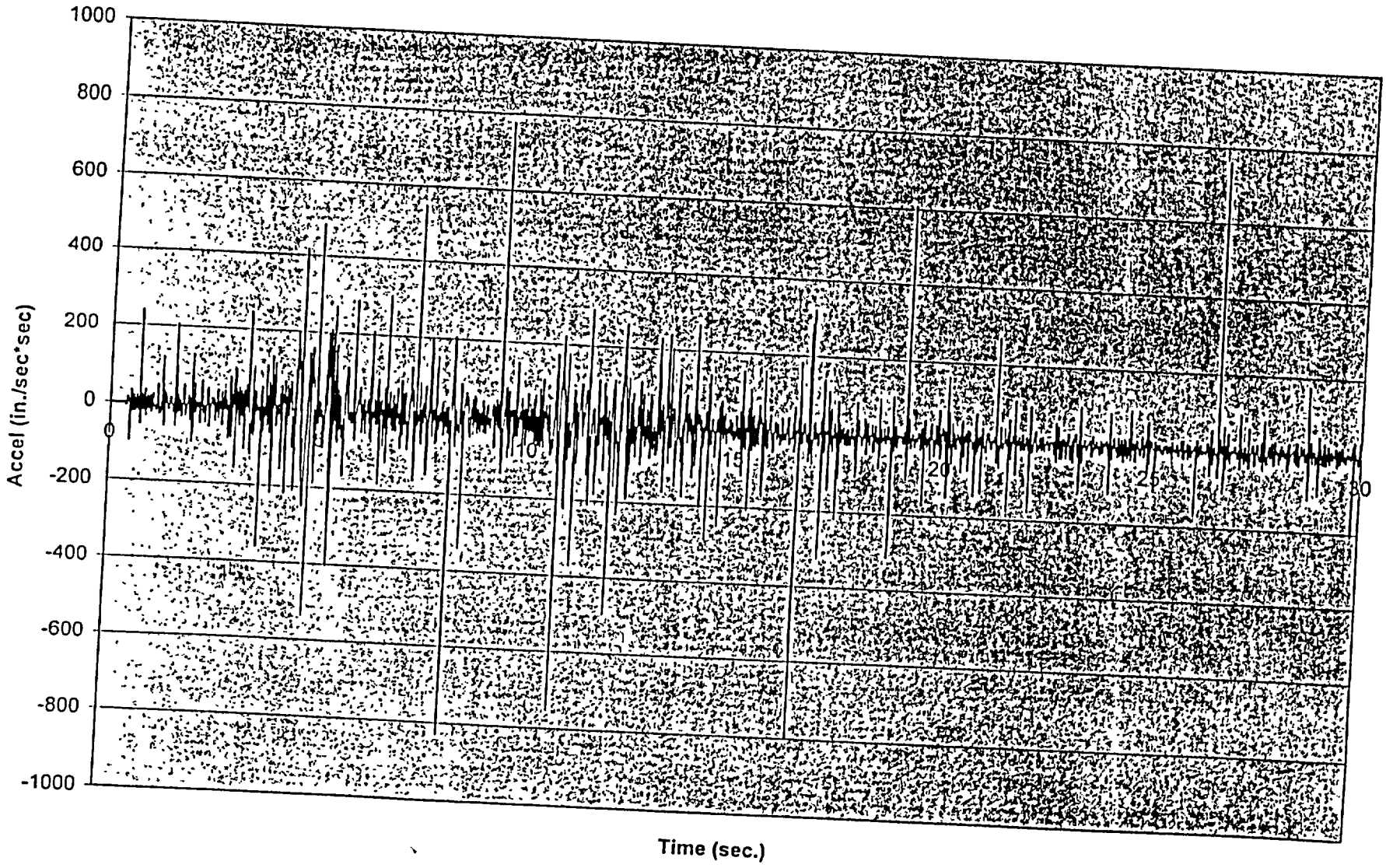

68248

Fig. 18 Cask 1 Accel-Y vs Time, cof 0.2 at point 2, file:pfs102

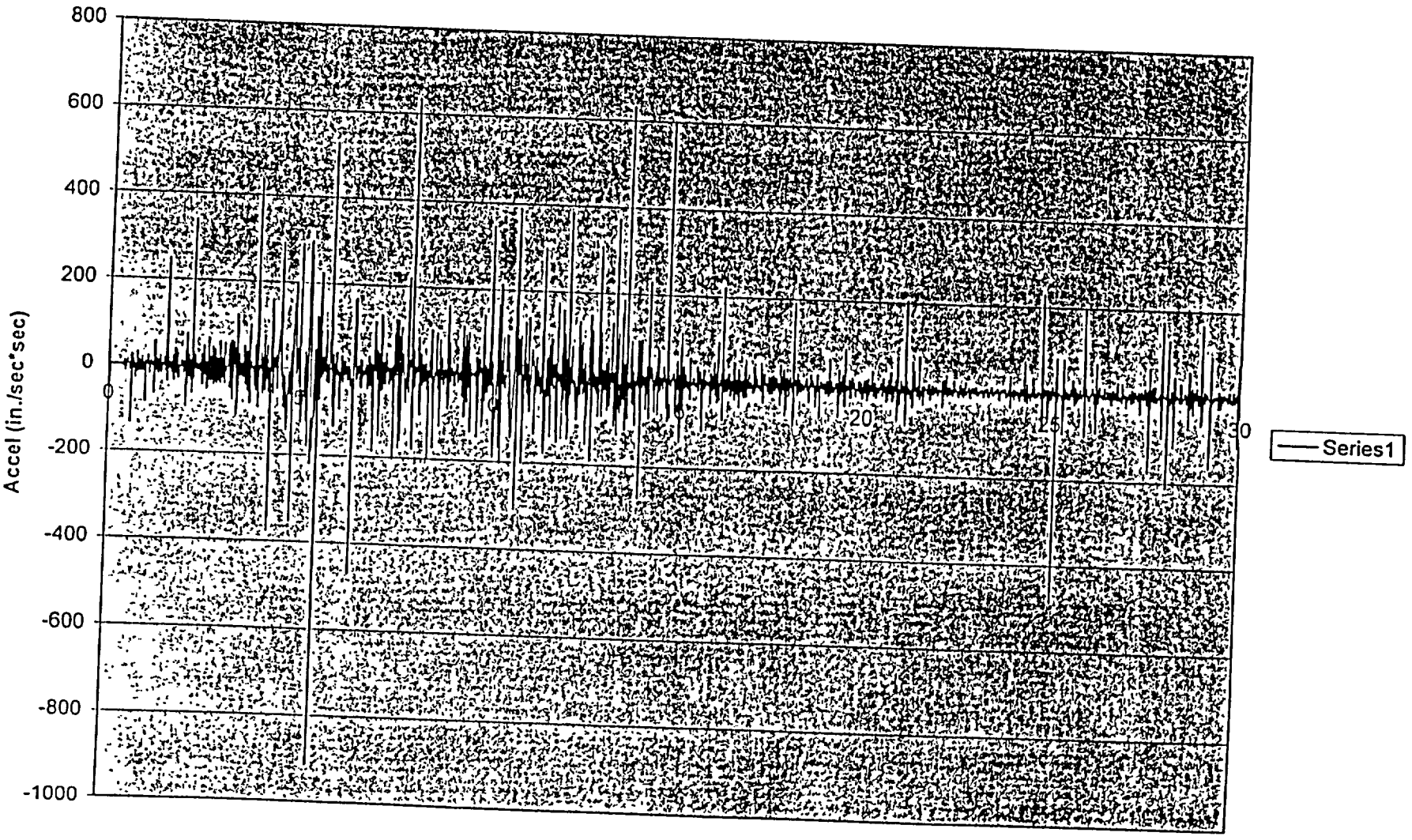

68249

Fig. 19 Cask 2 Disp-X,COF=0.2 at point 2, file:ck2disp2

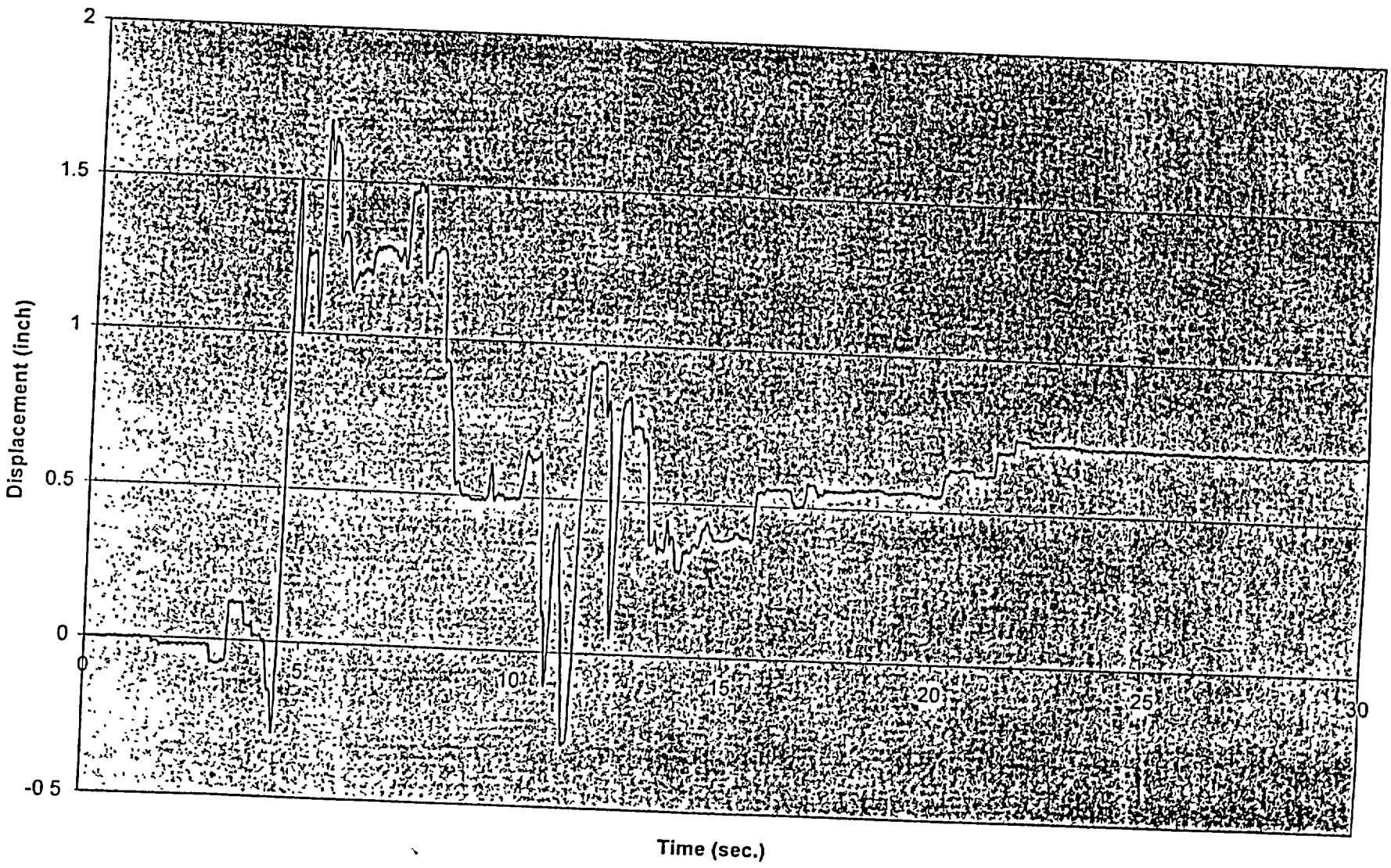

68250

Fig. 20 Cask 2 Disp-Y, COF=0.2 at point 2, file:ck2disp2

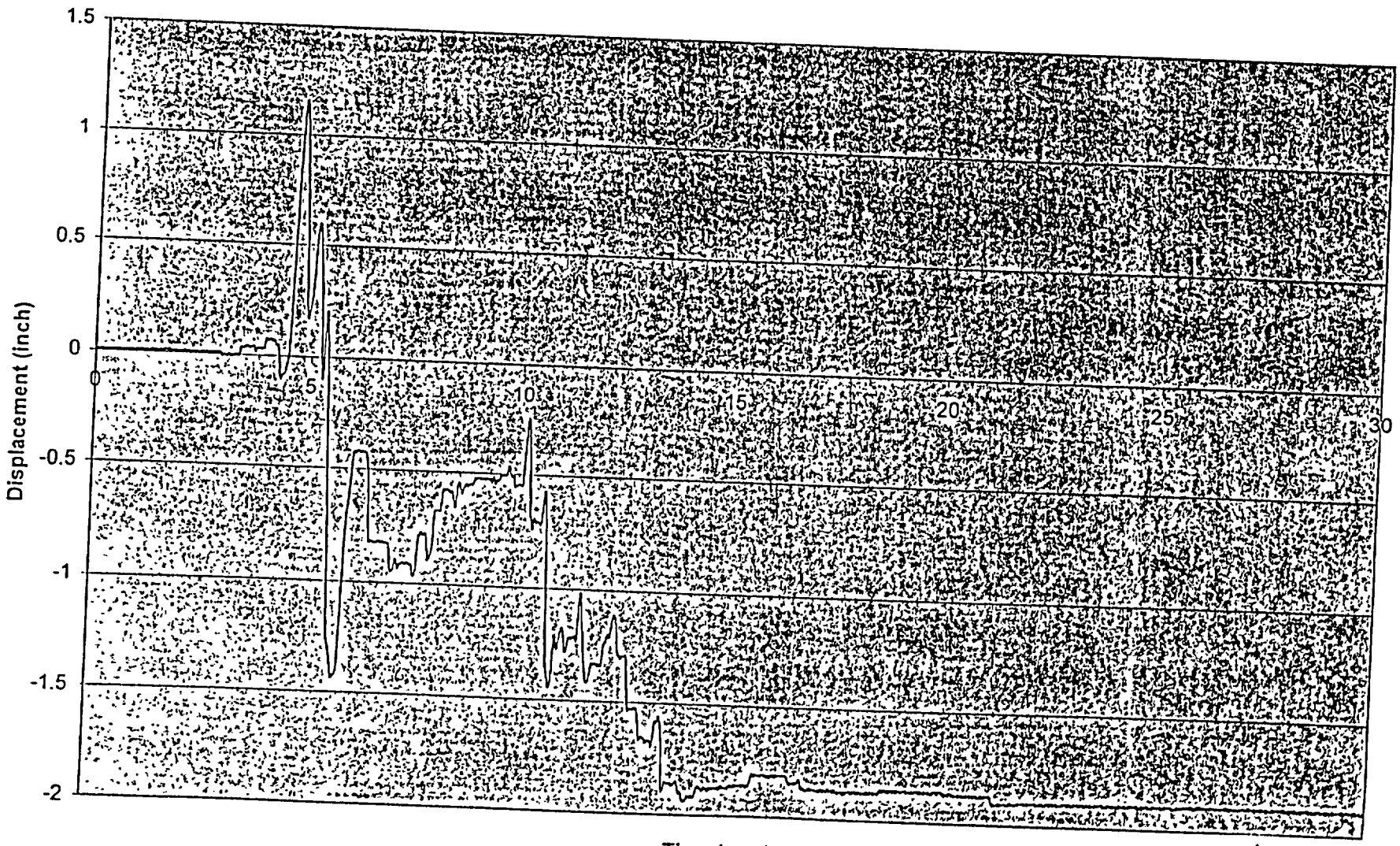

68251

Fig. 21 Cask 2 Vel-X vs time,cof=0.2 at point 2, file:pfs202

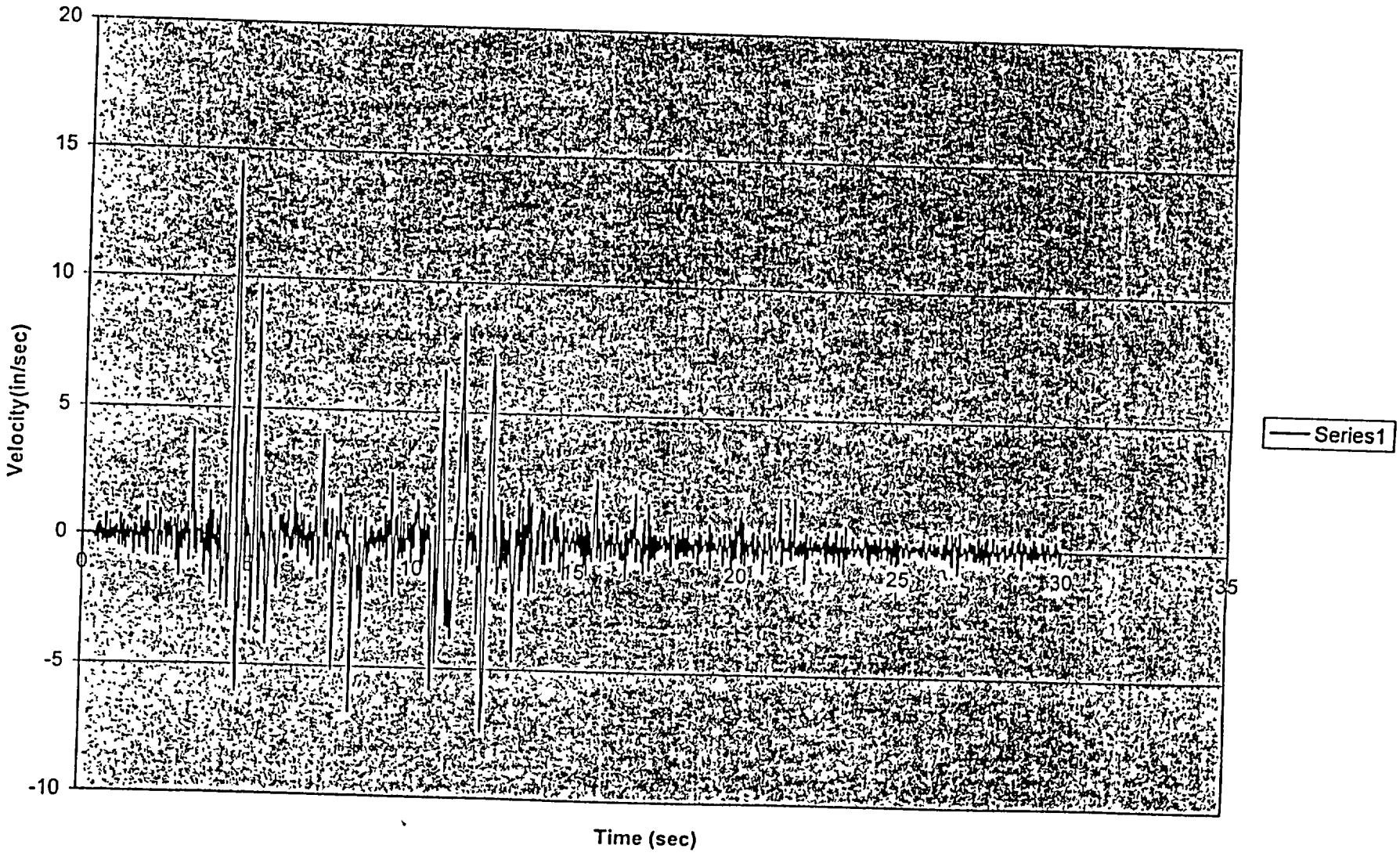

68252

Fig. 22 Cask 2 Vel-Y vs Time,cof = 0.2, file:pfs202

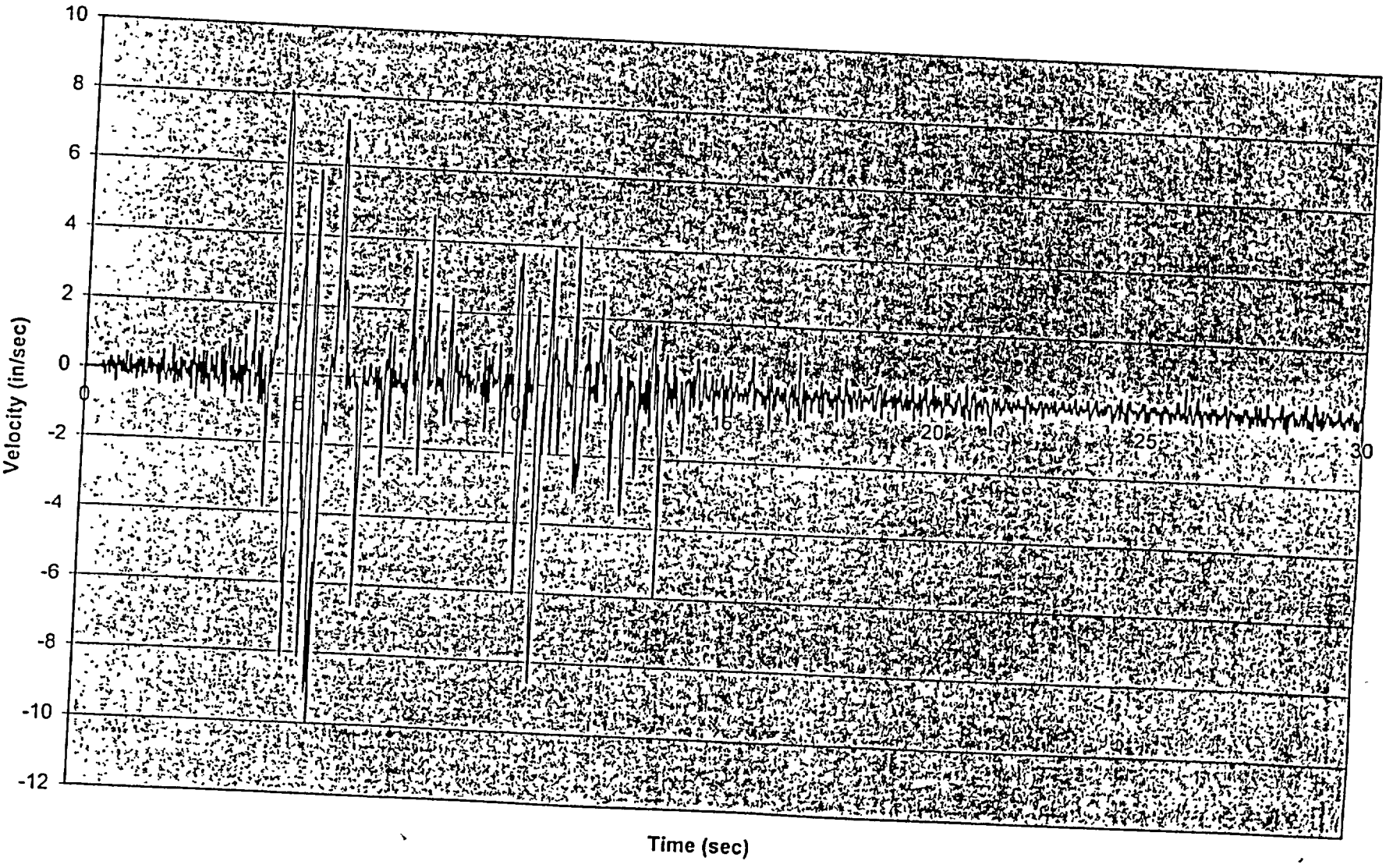

68253

Fig. 23 Cask 2 Accel-X vs Time,cof = 0.2 at point 2, file:pfs202

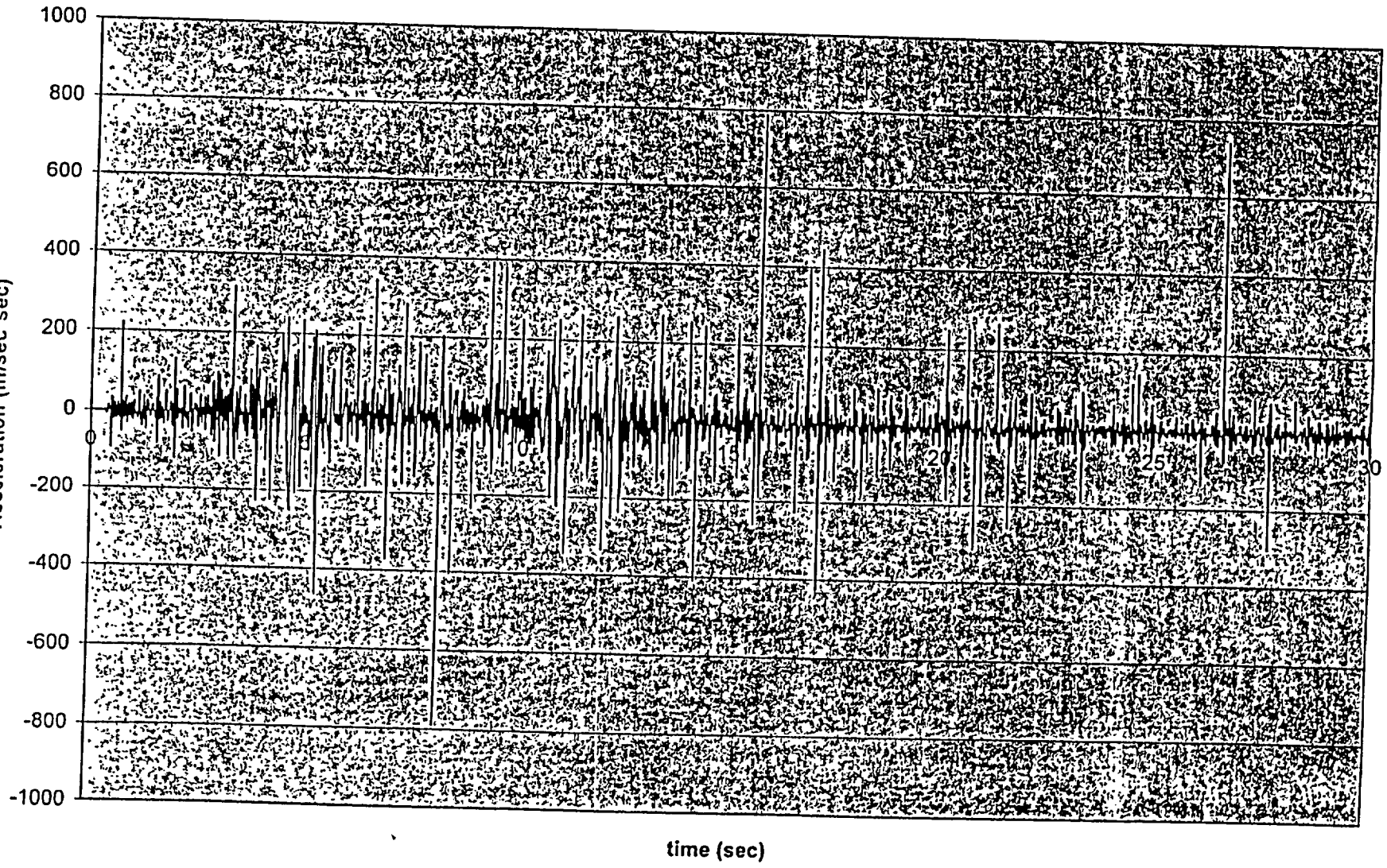

68254

Fig. 24 Cask 2 accel-Y vs Time,cof 0.2, at point 2, file:pfs202

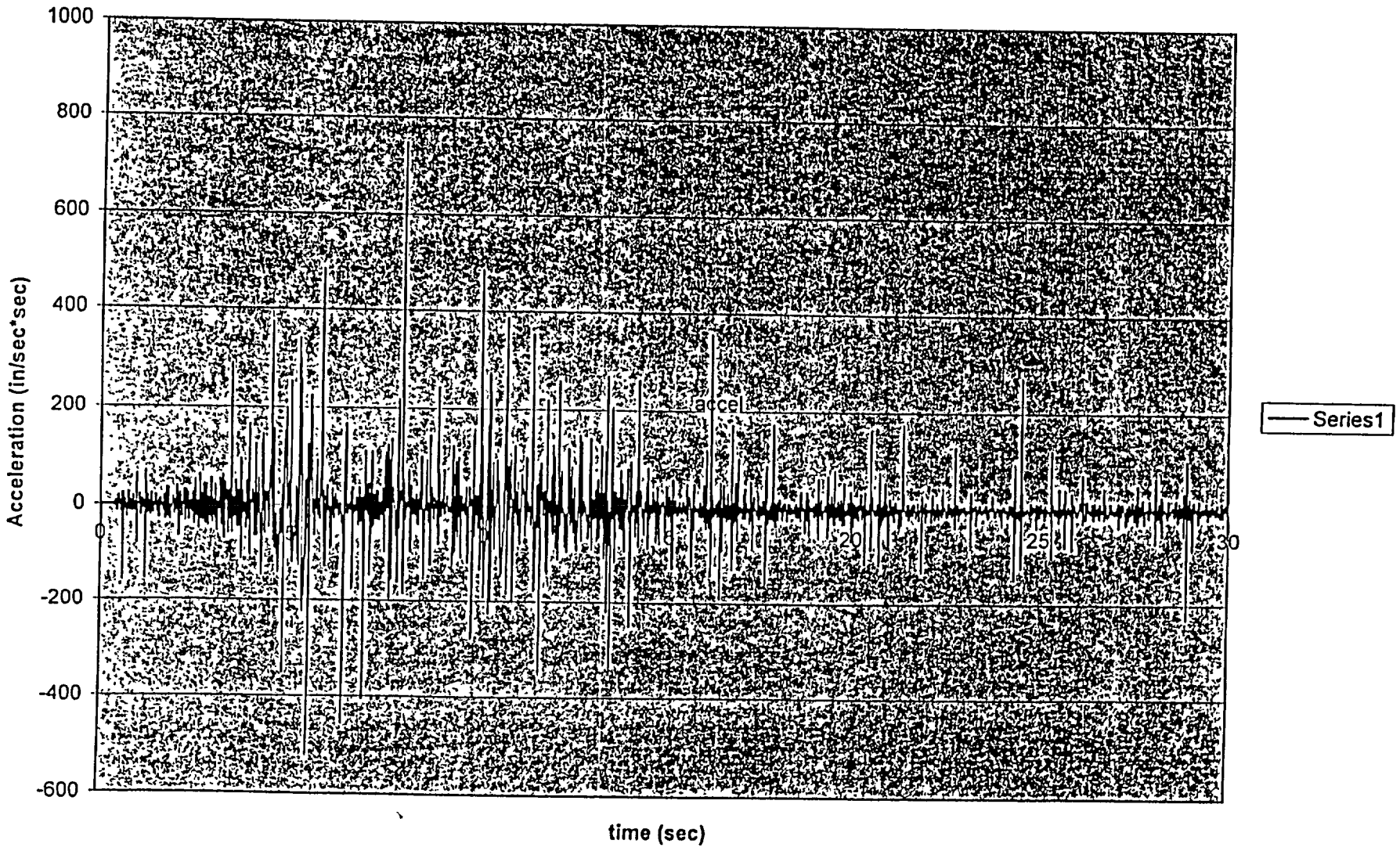

68255

[illegible] COMMISSION

[illegible] No. LL

[illegible] PTS

[illegible] IDENTIFIED ✓

[illegible] ✓ RECEIVED ✓

[illegible] REJECTED

[illegible] WITHDRAWN

DATE 9/29 Witness

Clerk